RL-TR-96-197
In-House Report
March 1997

APPLICATIONS OF OPTICAL GAIN MEDIA

Reinhard K. Erdmann

APPROVED FOR PUBLIC RELEASE; DISTRIBUTION UNLIMITED.

19970429 194

Rome Laboratory
Air Force Materiel Command
Rome, New York

DTIC QUALITY INSPECTED 1

This report has been reviewed by the Rome Laboratory Public Affairs Office (PA) and is releasable to the National Technical Information Service (NTIS). At NTIS it will be releasable to the general public, including foreign nations.

RL-TR-96-197 has been reviewed and is approved for publication.

APPROVED: James W Cusack

JAMES W. CUSACK
Chief, Photonics Division
Surveillance and Photonics Directorate

FOR THE COMMANDER: Donald W. Hanson

DONALD W. HANSON, Director
Surveillance and Photonics Directorate

If your address has changed or if you wish to be removed from the Rome Laboratory mailing list, or if the addressee is no longer employed by your organization, please notify Rome Laboratory/OCPA, Rome, NY 13441. This will assist us in maintaining a current mailing list.

Do not return copies of this report unless contractual obligations or notices on a specific document require that it be returned.

REPORT DOCUMENTATION PAGE

Form Approved
OMB No. 0704-0188

Public reporting burden for this collection of information is estimated to average 1 hour per response, including the time for reviewing instructions, searching existing data sources, gathering and maintaining the data needed, and completing and reviewing the collection of information. Send comments regarding this burden estimate or any other aspect of this collection of information, including suggestions for reducing this burden, to Washington Headquarters Services, Directorate for information Operations and Reports, 1215 Jefferson Davis Highway, Suite 1204, Arlington, VA 22202-4302, and to the Office of Management and Budget, Paperwork Reduction Project (0704-0188), Washington, DC 20503.

1. AGENCY USE ONLY *(Leave blank)*	2. REPORT DATE	3. REPORT TYPE AND DATES COVERED
	March 1997	**FINAL, Oct 92 - Sep 96**

4. TITLE AND SUBTITLE

APPLICATIONS OF OPTICAL GAIN MEDIA

5. FUNDING NUMBERS

C - NA
PE - 62702F
PR - 4600
TA - P2
WU - 07

6. AUTHOR(S)

Reinhard K. Erdmann

7. PERFORMING ORGANIZATION NAME(S) AND ADDRESS(ES)

Rome Laboratory/OCPA
25 Electronic Pky
Rome NY 13441-4515

8. PERFORMING ORGANIZATION REPORT NUMBER

9. SPONSORING / MONITORING AGENCY NAME(S) AND ADDRESS(ES)

Rome Laboratory/OCPA
25 Electronic Pky
Rome NY 13441-4515

10. SPONSORING / MONITORING AGENCY REPORT NUMBER

RL-TR-96-197

11. SUPPLEMENTARY NOTES

Rome Laboratory Project Engineer: Reinhard K. Erdmann, OCPA, 315-330-4455

12a. DISTRIBUTION AVAILABILITY STATEMENT

APPROVED FOR PUBLIC RELEASE; DISTRIBUTION UNLIMITED

12b. DISTRIBUTION CODE

13. ABSTRACT *(Maximum 200 words)*

The work done under this project number included a variety of projects over a period of several years and for this reason the topics are covered separately. One major unifying theme involved the practical applications of optical gain media in fiber optic systems. These followed somewhat of a logical progression in that optical amplification specialized to fiber amplification, which stimulated fiber laser development. Since some of these efforts at times overlapped and involved other personnel, this report emphasizes those areas not previously covered by other reports and even some topics not well covered in current literature. It can be observed in retrospect that many of the experiments in this project paralleled or preceded key developments in the fields of optical amplification and ultra short pulsed fiber based sources. To facilitate an overview of the several distinct project areas, the most important results of each one are summarized separately. Detailed experimental descriptions are given, and in some cases are supplemented by theoretical analysis of important aspects.

14. SUBJECT TERMS

semiconductor optical amplifier (SOA), fiber amplification, fiber lasers, modelocked fiber lasers, erbium doped modelocked fiber lasers

15. NUMBER OF PAGES

84

16. PRICE CODE

17. SECURITY CLASSIFICATION OF REPORT	18. SECURITY CLASSIFICATION OF THIS PAGE	19. SECURITY CLASSIFICATION OF ABSTRACT	20. LIMITATION OF ABSTRACT
UNCLASSIFIED	**UNCLASSIFIED**	**UNCLASSIFIED**	**UNLIMITED**

TABLE OF CONTENTS

LIST OF FIGURES

1.0 INTRODUCTION

The work done under this project number included a variety of projects over a period of several years and for this reason the topics are covered separately. One major unifying theme involved the practical applications of optical gain media in fiber optic systems. These followed somewhat of a logical progression in that optical amplification specialized to fiber amplification, which stimulated fiber laser development. Since some of these efforts at times overlapped and involved other personnel, this report emphasizes those areas not previously covered by other reports and even some topics not well covered in current literature. It can be observed in retrospect that many of the experiments in this project paralleled or preceded key developments in the fields of optical amplification and ultra short pulsed fiber based sources. To facilitate an overview of the several distinct project areas, the most important results of each one are summarized separately. Detailed experimental descriptions are given, and in some cases are supplemented by theoretical analysis of important aspects.

2.0 SEMICONDUCTOR OPTICAL AMPLIFIERS

A few comments should be made regarding the motivation for optical amplification in general. It is unavoidable that signals in real systems have loss and in general require either amplification or complete signal regeneration to compensate propagation or coupling losses. This can be done in either the electrical or optical domain. Since in fiber the signal is already in the form of light energy, it is advantageous for the processing to be done in this domain to avoid further coupling losses. Conversion to the electronic or optical domains induces excess loss, additional noise and significant component complexity. Furthermore, nearly every advanced interconnect or LAN configuration poses numerous splitting losses, which in turn require compensation in distributed systems. The unfortunate situation is that while most electrical amplifiers are generally compact and inexpensive, optical amplifiers are difficult to integrate and are very expensive. It is therefore necessary to assess their actual and potential performance in light of applications which would justify the special effort required by this technology.

Amplifier Noise and Mode Matching

A particular feature that applies to all amplifiers is noise, particularly noise generated by the amplifier itself, commonly referred to as ASE (amplified spontaneous emission). Figures 4,5 show the incident signal and the amplified signal riding on a background of ASE. This width corresponds to the spectral emission linewidth, which is on the order of 40 nm for most diode and fiber based amplifiers. It will be seen, of course, that a semiconductor optical amplifier (SOA) still requires some waveguide-fiber coupling considerations due to the mismatched mode field overlap. Nevertheless, a SOA possesses several unique potential advantages. In particular, the small size allows cascaded and integrated devices, and in some cases even monolithic integration. Since a semicionductor traveling wave amplifier (fig. 15) is based on a diode laser with facet reflections minimized, the basic technology was developed earlier than rare earth doped

fiber designs. When this particular work was in progress, doped fiber was only available on an experimental basis, and even semiconductor amplifiers had to be custom made or purchased in prototype form at costs up to 20k. The active gain chips used were provided for cooperative experimental purposes by GTE laboratories (fig. 15). The optical fiber coupling, applications and performance analysis were done at Rome Laboratory.

Purposes of the Experimental Work

1. Assess the overall practicality of this type of amplification
2. Measure the short pulse performance response implications

At the time of this work, almost no high speed-short pulse response testing had been performed anywhere on such devices. Some of the results given here were presented at OSA in Boston 1990. Later, measurements were performed on devices of their own fabrication at AT&T Bell laboratories and at British Telecom. These largely collaborated the results and provided some additional details. The key results are summarized; experimental details and data are provided subsequently.

Experimental

The first set of experiments involved straightforward gain and coupling efficiency characterizations. These were necessary to assess the cw performance of the traveling wave laser gain diodes provided by GTE labs, and also to develop coupling methods for lab use or eventual packaging considerations. Such measurements had been made at GTE and data was available for comparison. The goal and new feature of the in-house work was the characterization as a pico second signal pulse amplifier and the determination of suitability for high bit rate applications. Though GTE was in general very well equipped, particularly for fabrication, this work was largely outside their capability. Access to pico-second optical pulse sources at 1.3 μm was at that time established in only a few laboratories in the world. The development of the externally pulse compressed and modelocked Nd YAG laser had just been completed at Rome Laboratory prior to this project. Its operation is more fully described in other technical reports. For the purpose of this work the key feature provided was a source of 1.5 pico-second pulses. The repetition rate was 100 MHz and the maximum pulse power was 10 pico joules.

There were three critical types of measurement required:

1. Determination of pulsed gain and amplified pulse shape
2. Net gain as a function of pulse power to find the gain saturation level
3. Determination of the gain recovery time constant

The test configuration used for this process, illustrated in figure 1, is known as a pump-probe setup. Establishing this required several new developments.

Fiber Coupling With Lensed Fibers

It is worth mentioning that in the course of this work experimental lensed fibers were produced at Rome Laboratory. This was done by placing a fiber segment under tension with a calibrated weight, and then applying heat from the Arc Fusion Splicer to a location near the other end. The separation induced by the arc melt resulted in a tapered fiber end with an approximately spherical radius on the end of the fiber core. The radius could not be measured directly but its performance and effective mode field size could be inferred from coupling measurements taken in autocollimation. This method of lensing the fiber was fairly difficult to control or to maintain consistently. Typically, more than a half dozen attempts were required to obtain a usable fiber lens. A Japanese manufacturer had invested in the tooling to accomplish lensing in a controlled manner. They actually embedded the fiber in a matrix and then polished the fiber tip to a controlled radius. In fact various radii became available. Since we were using these fibers as a means to an end, lensed fibers for this and subsequent work were purchased from this vendor. A simple fusion splice then provided coupling into the system under test. These fiber ends were also metalized, which facilitated the soldering required for permanent packaging.

Waveguide Coupling

The main consideration is coupling into the chip with lensed single mode fibers. Those purchased from Kyocera had a tip radius of curvature of 10 μm. Because of the angle stripe geometry of the waveguide (fig. 15), an ordinary cleaved fiber cannot be butt coupled, since the gap between fiber and waveguide ends is much too great for efficient coupling These lensed fibers were characterized for loss in this configuration and compared with microscope objectives in end-fire configurations. The latter implies that a lens is positioned at its focal distance from the waveguide end, resulting in a nearly collimated output. Although an objective could capture nearly all of the light in this manner from the waveguide, it was possible to re-focus only about half of this into a single mode fiber. This was very close to the same net efficiency the lensed fibers achieved without any bulk optics whatsoever. Furthermore, the lensed fibers could be aligned and permanently fixed in a packaged device. Packaging is, however, an involved procedure, requiring sub-micron precision alignment as well as ultra-stable retaining methods. The method developed at GTE Laboratories involved a special two-stage solder. Other labs have worked with epoxy retainers, however these generally lacked long term stability. The problems are due largely to thermal mismatches and mechanical instability of epoxy if the volume is not properly minimized. For the purposes of our experiments, alignment stages for holding fiber was more than adequate, and our tests confirmed similar performance results on packaged and unpackaged amplifier devices.

Electrical Power and Bonding Methods

The non-packaged versions required that one bring a current probe to the contact pad, which had been wire-bonded to the metalized chip surface. In the course of this work, experience was gained in the use of both conductive epoxies and wire bonding. The former utilizes silver metal embedded in an epoxy matrix, and cures with heat. The epoxies work well for larger devices, whereas small chips require soldering to be applied in a full scale solder/bonding station. This type of equipment was acquired at Rome Laboratory recently. For the wire bonding, a specialist was brought in for a day to give instructions in wire bonding techniques on our equipment. The metal mount also had to be placed in contact with a thermo electric cooler for operating temperature setting and stability. The gain level decreased with increasing temperature due to thermal depopulation of the conduction band energy levels participating in the gain population inversion. The practical limit on the lowest convenient operating temperature is set by the capacity of the TE cooler. It is also necessary, however, to avoid possible condensation on the optical waveguide surfaces by maintaining a temperature above 0 °C in a normal atmosphere.

CW Gain

To determine the continuous operation (CW) gain, the fluorescing waveguide was electrically driven and the optical output was measured with a free space power meter (fig. 16). With care to assure that the detector size exceeds the exit beam size at a given distance, this method guarantees absolute detection capture of all the emitted light. When these measurements are repeated with lensed fiber in place, the difference gives the lensed fiber coupling loss. With this calibration established, a small input signal is inserted in one of the coupled fibers. The resulting output can be used to determine the **small signal gain**.

Saturation Power

When the input signal level is systematically increased, eventually the output signal ratio becomes nonlinear, thereby establishing the **saturation output power**. These two measurements are essential to determine application suitability. It is surprising how many engineers attempt to use a small signal gain amplifier (electrical or optical) with an input signal level that exceeds the saturation output power. The power gain in such a case is always less than the small signal gain and may even approach zero dB gain. For this reason electrical amplifiers are commonly classed as pre (low power), medium, or high power amplifiers to define the saturation power level. Optical amplifiers have not yet reached such standardization. The saturation power potential is quite different in a semiconductor optical amplifier (SOA) being analyzed here, as compared with fiber optic amplifiers which are described in the following sections of this report. It will be seen that in a SOA the saturation optical output power is related to the pump current and is typically a few milli-watts, limited by current carrier to waveguide dimensional

confinement factors. In a fiber amplifier the saturation power is determined by the optical pump power. This can in practice approach a Watt , and with 20% to 50% conversion efficiency, a properly optimized system can yield hundreds of milli-watts saturated power. This several order of magnitude increase is one of the reasons fiber amplifiers have been successfully implemented in systems.

For the SOA analyzed in this work, a typical input signal (fig. 3) is 2 micro watts, realizing a small signal CHIP gain of 20 dB just prior to the onset of gain compression. The net gain of 10 to 12 dB would in itself still be suitable for applications such as switching, coupling and distribution loss compensation. The foregoing considerations apply to the CW case, and several other issues become important in pulsed applications. The primary interest in amplification was the performance as a high speed short pulse optical amplifier. The characterization of pulsed response is more involved and several effects must be distinguished. Gain is equally important in both cases. The additional factors that come into consideration which do not appear in simple CW applications are:

a. **Pulse shape integrity**
b. **Gain recovery**

The first factor ensures that all portions of the pulse (high and low intensity) are amplified linearly. In particular, the output pulse has the same temporal (and spectral) width as the input. Gain recovery is discussed immediately after the next section.

Description of Short Pulse Laser Source at 1.3μm

At this point it is appropriate to describe in more detail the input pulse source. This is a modelocked Nd Yag Laser with end mirrors coated for the 1.319 μm line. Because the spectral bandwidth of this line is very narrow, the transform limit permits pulses no shorter than about 90 pico-seconds (ps). These are then compressed externally in a configuration which has been described in other Rome Laboratory technical reports and has also become a "standard technique". In brief, the high peak power of the pulse generates the nonlinear effect of self-phase modulation. The induced temporal index variation in the medium (optical fiber) results in a frequency chirp manifested as a spectral broadening of the pulse energy by several orders of magnitude. By passing through a proper dispersive device (diffraction grating pair) the velocity mismatch due to group velocity dispersion can be compensated. Then the leading "red" edge and trailing "blue" edge of the spectrally broadened pulse can be made nearly coincident. The result is a compression of the original pulse by up to two orders of magnitude (a factor of about 75 in this case.) The temporal and spectral pulse measurements of input and output confirmed that there was no observable width change(fig.6). This is excellent news from an applications view, indicating that picosecond pulses can indeed be amplified without distortion. From a theoretical point of view this is to be expected since the fundamental amplification process is based on stimulated emission having a time constant in such semiconductors in the femto-second (fs) range. It is nevertheless essential to verify this

experimentally to confirm that there are no other temporal broadening mechanisms overriding this.

Gain Recovery Time Constant

Since distortion-free amplification of short pulses can be accomplished, the key question presents itself. How closely spaced can such pulses be to still allow the medium time to either recover its full gain performance or maintain it at a constant level? An incomplete recovery would generate what is called inter symbol interference, or gain dependence on preceding states. This is because in a digital application (fig.2) for example: a number of "ones" in the signal preceding a given slot, will incur a different gain recovery than one having a number of "zeros" before it due to non-uniform recovery. The characterization methods suitable for this fall into two groups.

The first involves system simulation methods such as bit-error-rate testing (BERT). This is effective in evaluating probable system results but not suitable for determining the causes. Any analysis is further complicated by having to consider the detailed BERT characteristics, particularly modulators and other components that it controls.

Pump-Probe Method

The measurement technique used here was more appropriate at this stage of the development testing. It is the aforementioned pump-probe analysis (fig. 1). The method involves sending a pulse "pump" into the amplifier, followed by a second (probe) pulse at a delayed time interval. This delay is accomplished by splitting the beam and inserting a retroreflecting mirrored translation stage in the free space portion of the system. A 10 ps delay then corresponds by the velocity of light in double pass to about 3 cm. Actually periodic trains rather than single pulses are injected into the amplifier. However the 10 ns modelocked pulse separation far exceeds all other relevant time constants in this experiment, and can therefore be ignored. The gain experienced by the probe pulse is then monitored as a function of delay time separation (τ). The elegance of this method is the fact that no fast detectors of any kind are required. The time delay is continuously adjustable between the pump and probe pulses, and is controlled by a moveable mirror adjustment to the path length of one arm. When the pump and probe signals are sent in orthogonal polarization states, a polarizing beamsplitter at the output allows the signal level detection to be simply performed in an averaged CW mode. This is in principle simple, but becomes more involved in optical fiber, which forms the coupling pigtails on some devices. Previous tests accomplished this in a much simpler space version. An incident state of polarization in a fiber generally evolves to a different state due to birefringence and coupling effects. This implies that linear input polarization does not remain in a rotated linear form, but rather elliptical, thereby producing crosstalk and interference at the output. With short lengths this effect may be minimal, but the two polarization axes must still be located upon exit. Such effects were indeed observed.

They were not fully analyzed because it would have taken the focus too far afield at the level of understanding available at that time.

Data Analysis I

A careful examination of the data (fig. 7) shows that full gain recovery requires about one to two hundred pico-seconds. This would indicate a maximum digital data rate on the order of ten gigabits per second, a rate which has only recently been approached in practical systems. The ultimate limitation to the recovery time mechanism is definitely a population effect, since charged carriers in the conduction band must be replaced. With the exception of customized material, ultra low capacitance or extraordinary bias levels, this time constant is typical of what has been measured in related materials. It should also be noted that a numerical fit to the data actually shows two time constants at work (fig.9). The longer one has been described, but the other is much faster, at hundreds of femto seconds, but does not extend to full recovery. (fig. 8,9) The mechanism for this one is not as well understood, but it has been ascribed to very fast local thermal carrier dynamics. Examination of the traces shows that a small part of the gain is immediately recovered. Thus distortion-free signal propagation still requires several hundred ps.

Pulsed Energy Saturation

A simplified two level model is useful (fig. 10) to illustrate the causes of gain saturation or compression. The previous discussion has been in the small signal regime. This means that there are a sufficient number of carriers per unit length so that number of photons (energy) in the input pulse times the gain, integrated over the total length, will not at some length deplete all the available carriers in a local region of the medium. When this takes place, the net gain(G) will no longer be equal to $e^{(gL)}$ but will instead be necessarily "compressed" to a lower value. The gain compression can be seen to be proportional to the input pulse energy.

One can define gain (g) as being proportional to the number of photons generated by a single photon, within a unit length in the gain medium. It should be noted that this definition differs significantly from the gain saturation mechanism in the CW case.

Data Analysis II

The small signal gain is seen to be essentially the same as the CW case as would be hoped. The gain saturation however, is completely different in nature and begins at a significantly lower level of average power than the CW case. The basic reason for this is again apparent from the two level model. Any input pulse can be seen as initiating a chain reaction of photon generation due to amplification, which takes place as a function of distance in the direction of propagation. At some distance along the amplifier length, the [number of photons/unit length][**x**(small signal gain factor], will exceed the population inversion per unit length. At that point gain saturation (compression) begins. This effect should clearly be proportional to the initial pulse energy, since that determines

the number of photons at the starting point of the amplifier (distance= zero). In practice of course the amplifier length is always finite so gain saturation does not occur until a certain value of pulse energy, which reaches the critical population density condition corresponding to the amplifier's given length. After that point the gain compression will be proportional to the initial pulse energy. The significance of this for applications is that low rep rate pulse trains (even single pulses!) can incur gain saturation regardless of how low the average power level is in the incident signal. The saturation energy is generally specified at the 3 dB gain reduction level, and is best measured experimentally. (fig. 4)

Non Linear Gain Effects

It should be noted that based on this model, there is no effect on gain predicted by high peak power intensity. i.e. If a pulse of given energy is compressed temporally with a corresponding increase in peak power to keep the energy constant, the gain saturation incurred would be unchanged. What in fact would occur is the eventual onset of observable non-linear optic effects, which respond in proportion to peak power rather than energy. Such effects were outside the focus of this particular study and are treated elsewhere. It is good news from a systems point of view, that high data rates(shorter pulses) can be sustained without compromise of gain. This is not so for higher energy pulses, and care must be taken to maintain uniform gain so as to avoid nonlinearity.

Polarization

Because of the significant asymmetry of the waveguide design, the gain was reduced by more than an order of magnitude in the TE as compared with the TM polarization. This was experimentally confirmed and all input signals were aligned to the favorable polarization. The output signal from our test source and laser diodes in fielded systems, are in general already highly polarized, so no additional loss is incurred if the alignment is proper. It would of course be very convenient not to require alignment or polarization control. The bi-refringent "paddle" polarizers used for this purpose are described in detail in another Rome Laboratory Technical Report. There are in fact design methods which have been explored subsequently to make the response polarization independent, but in general the resulting sacrifice in the gain performance did not justify these. Though this posed a limitation, it was not the most critical one. It will be seen that fiber amplifiers avoid this problem by having a symmetric waveguide with a polarization independent response.

Experimental Summary

1. The amplifier responds on a time scale of about 1 pico-second. This would in itself indicate suitability for high speed applications (fig. 2) with an upper limit of about 100 Gigabit per second data rates, **if** the recovery time were on the same order.

2. The actual chip gain is about 20 dB. but a maximum of only about 14 dB is realizable fiber to fiber. The response is very highly polarized and requires proper attention to orientation. This gain is sufficient for some practical applications.

3. The gain saturation has two independent mechanisms.
   The *CW* 3 dB saturation power is approximately 1 mw.
   The *pulsed* saturation energy level is proportional to the pulse energy.

The 3 dB saturation level is about 1 μ Joule. This means that regardless of average power, even a single pulse could incur saturation yielding signal non-linearity. These devices are therefore suitable mainly as low power or moderate pulsed energy amplifiers.

4. The gain recovery time is on the order of 100 pico seconds to nano-seconds. This poses some serious system implications which are described later in more detail.

5. The net modal insertion loss is about 4 to 6 dB. This value is subtracted from the chip gain to yield the net fiber to fiber gain.

6. Packaging and lifetime considerations were largely equivalent to packaged diode lasers, a technology that is relatively well developed.

Conclusions and Implications for Future Work

Although they functioned reliably to the specifications described, the limitations of semiconductor optical amplifiers generally outweighed their utility. The dynamic range in a standard in line configuration is an order of magnitude less than a fiber amplifier. The most critical shortcoming was that no solution exists, short of new material development, to the performance restrictions imposed by the gain recovery time constant. The fact that the gain varies over a time period of 10 to 1000 ps, causes significant inter-symbol variance. The gain experienced by sequential signal pulses varies, causing crosstalk from uneven gain recovery. It will be seen that ironically this problem is not present in fiber amplifiers due to the very long recovery lifetime on the order of milliseconds. The TWLA amplifiers used for this analysis were provided by GTE Laboratories. The only other manufacturers at that time were ATT Bell Laboratories and British Telecom, which marketed some at a very high price through BT&D. One such was in fact obtained by another group in Rome Laboratory. All of the analysis and principles here described applied almost universally to these as well even though there were a few distinctions. The other two manufacturers did not use angle stripe geometry for reflective feedback suppression, but rather anti-reflection coats which had to be very precisely optimized. Their waveguide gain stripes were somewhat narrower and hence the confinement factor allowed lower threshold and operating currents (<100 ma compared with 300 ma) in a particular configuration. The tradeoff was that they had lower saturation power levels.

In subsequent years MQW designs became available, and further increased confinement factors. Both the characteristic advantages and shortcomings remained essentially the same for all manufacturers designs. The significant limitations resulted in the follow on research thrust to be directed in the areas of optical fiber amplifiers. This was prior to the time when fiber amplifiers became successfully developed and deployed in long haul links and underseas cable. In summary, a diode laser amplifier was established as being suitable for very short pulse amplification. The performance constraints were, however, very significant and limiting. Net gain, gain saturation, gain recovery were about an order of magnitude off from values required for practical system deployment.

3.0 EXTERNAL CAVITY SEMICONDUCTOR LASER SOURCE

An external cavity laser design, based on an angle stripe traveling wave semiconductor amplifier (TWLA), was designed, constructed and characterized. The purpose here was to assess its utility as a flexible signal source incorporating several key operating characteristics, that could not simultaneously be met by any existing sources. These are:

Key Design Features

1. Compatibility with single mode fiber systems
2. Convenient wavelength tuning
3. Capability of generating short pulses at variable repetition rates

It is demonstrated in the following experimental work that these requirements can largely be met by the systems illustrated in figures 14 and 15. The gain medium is formed by an InGaAsPh ridge waveguide in an angle stripe geometry. The waveguide itself was designed and fabricated by GTE Laboratories and provided to Rome Laboratory for experimental work. Its internal gain of up to 25 dB, and its performance as an in-line short pulse optical amplifier, have been described in the previous sections. The angled geometry suppresses undesirable reflective feedback to less than -40 dB without requiring an ultra-critical (Rx<.01%) anti-reflection coating. Several of the chips used in these devices were AR coated to moderate tolerance only to reduce losses. The lasing action was achieved on a selection of these chips with or without such coatings.

Cavity Coupling Methods

The laser cavity itself was configured by end-fire coupling to the waveguides with 20 x microscope objectives (AR coated (@1.3μm), which yielded about 50% coupling efficiency. This limitation is typical of an asymmetric waveguide collimated by good quality spherical optics. The standing wave cavity was formed by the two plano end mirrors, one a dielectric max reflector (Rx>99.5%) and the other an 80% output coupler. Lasing was readily achieved as well in two other configurations. The first method generates a collimated beam incident and reflective from the end mirrors. The second one is commonly referred to as a "cat's eye" configuration Retroreflection is achieved by

coming to a point focus thereby inverting the beam about the optical axis. It can be shown theoretically that this produces a more stable cavity and is also relatively insensitive to small misalignments. Remarkably this design also resulted in greater output efficiency.. For similar reasons, even cavities designs having no need for collimating optics seldom utilize plano end mirrors. A relatively long concave radius has superior stability.

Pumping Techniques and Power Output

The drive current was held near the threshold value of 200 ma at a temperature setting of 14.5°C, which was maintained with a closed loop thermo-electric cooler. Figure 16 gives the IV characteristic data. The CW output was 500 microwatts centered at a free running wavelength of 1.33 μm.(fig. 17). With the replacement of the end mirror by a 600 groove/mm diffraction grating optimized near that wavelength, the output could be tuned over about 20 nm or half of the fluorescence gain bandwidth. At the peak of the gain the power output dropped only about 1 dB as compared with the mirror. This is due to the fact that the waveguide output is polarized and is matched to the "S" polarization response of the grating.

Fiberized Version of the Laser

A nearly all fiber version of this cavity was subsequently assembled. The motivation was to eliminate the bulk of the free space optics, and also to eliminate the need for most of the optical alignment. The coupling was done with single mode lensed tapered fibers, displaying similar coupling efficiencies to the free space version. One end mirror was formed by a vapor deposited gold coating directly onto the cleaved fiber end. The other was formed by a 90/10 % dielectric partial reflector. This required input and output collimation by integrated gradient index lenses, which are extremely compact. It is apparent that this configuration very much resembles a true fiber laser. The direct electrical pumping is very convenient, but the drawbacks of semiconductor amplifiers are still present. These can generate undesirable effects such as gain dependent frequency chirp in the output signal. For this reason work on a fiber version was terminated.

Modelocking

The pulsed operation for optical signal processing applications was achieved by two modelocking methods. It should be mentioned that gain switching or self relaxation oscillation was not done. The reason being that these approaches are already in established use, and are known to have fundamental limitations in terms of frequency chirp content as well as limited short pulse temporal response. It is established that modelocked pulse generation can solve both of these limitations. The experiments were required to demonstrate this in an external cavity diode laser at the wavelengths required for fiber optics applications.

Active / Passive Performance Comparison

It was deemed very important to establish the relative stability advantages of active versus passive modelocking in this configuration. Experience with other types of lasers would indicate that active methods in general provide greater control with longer pulses , while passive methods yield shorter pulses from simpler cavity designs. To the best of our knowledge, no prior experiments anywhere had directly compared the amplitude and timing stability of these two fundamental modelocking methods in such a cavity. This study achieved some fundamental significance.

Active modelocking was established in the conventional manner using direct drive current modulation. A bias T was used to combine a 17 dBm sinusoidal RF signal from a high quality frequency synthesizer (HP 85607B) with the 200 ma bias current. The 0.5m cavity length corresponds to approximately 300 MHz; however the second harmonic at 600 MHz was chosen to optimize the tradeoff for a high data rate single channel, which could still utilize readily available electronic processing equipment. Another consideration was the fact that the small signal response of the TWLA chip in this connectorization indicated falloff at frequencies greater than 1 GHz.. This was measured directly using a frequency synthesizer and a 3 GHz detector.

Temporal Measurements

Measurements on the pulses were taken with a high speed detector/ oscilloscope combination. These were an Antel ARD 28 (15 GHz photodiode) and a Tektronix 8705-50Ghz scope head with a combined system impulse response FWHM of 40 pico-seconds. (fig.18) This produced a modelocked pulse train display with halfwidths of 48 ps. This system is even now near state-of-the-art for direct measurement capability. Shorter pulses are measured on an autocorrelator which can resolve to femto second ranges, but at the sacrifice of some shape and timing information. In this particular range we were able to use both instruments to confirm the results with great certainty. The autocorrelator here was a background free model (Inrad diode laser model 678). The scope data indicates complete suppression of any satellite pulses. In some other reported systems, these have been seen to build up to substantial energy levels from even small residual facet reflections.

The ultimate limit to the pulse width is set by the Fourier transform shape factor for the spectral profile (fig.17) which for 40 nm would permit widths as low as tens of femto seconds. This limit is not in general attained for several important reasons given in the section following data analysis.

Theoretical Data Analysis

The shortest pulses obtained from diode lasers can be more than an order of magnitude greater than those observed here. The modelocked spectral data given in (fig 17) is

considerably narrower than 40nm. Other factors pertinent to this experiment are described in the following.
The theoretical pulse width for steady state amplitude modulated modelocking is given by :

$$t = 0.45\left(\frac{g}{\Delta m}\right)^{1/2}\left(\frac{1}{f * \Delta fa}\right)^{1/4}$$

If one uses the following values of the parameters:

f = 300 MHz (Signal Frequency)

Δf_a = 1.5×10^{12} Hz (See fig. for mode-locked spectral data indicating $\Delta\lambda$=10nm)

Δ_m = 0.2 (modulation depth based on electrical drive values)

g = 1 (Round Trip Gain)

Then **(t),** the measured pulse durations are in reasonable agreement with the theory, and exhibit an approximate $sech^2$ shape. We note that a much shorter cavity length with the corresponding higher drive rate such as 30 GHz (corresponding to a 5 mm long cavity), would dictate a reduction in the actively modelocked pulse width by a factor of 10. This has indeed been demonstrated. For many applications such as this one, however, the frequency needs to be kept lower than several hundred megahertz.

Applications

In certain applications such as synchronous TDMA (fig.2), even pulses of the widths exhibited here could support aggregate data rates of up to 10 gigabits, with individual channels running at the repetition rate of 600 gigabits. A diode laser based structure such as the one described presents numerous benefits: an extremely compact gain medium and very simple pump delivery. Furthermore the high energy conversion efficiency, reliability and lifetime make this potentially suitable for a field device. There is also an advantage in temporal stability compared with many other laser types.

Performance Features

1. The rate is adjustable via the cavity length.

2. High saturation power versions of this module are under development.

3. The timing jitter is lower than many other sources.

The last of these warrants further examination because in the limit of very short pulses, it becomes the ultimate limitation to system signal rate. Discussion of this subject is included in the last section with frequency noise measurements.
Decreasing the temporal pulse width clearly increases the total information rate capacity in the absence of other overriding factors. It also improves the temporal resolution for probing material or device response characteristics. This can be accomplished in diode lasers even at low repetition rates by various methods falling into three main groupings.

1. Direct modulation, including gain switching, and relaxation oscillation effects.

2. Passive modelocking via a saturable absorber such as an MQW or a specially modified gain/loss region.

3. Active modelocking with extremely short electrical control pulses.

Hybrid combinations of these can also be effective, and pulse compression methods such as those based on dispersion/chirp compensation can be applied within or outside the cavity.

Regenerative Modelocking

For this set of experiments we chose a particular method termed regenerative modelocking (fig.14). In this approach the longitudinal cavity modes themselves provide an optical signal, which is first detected, then electrically amplified prior to being "fed back" to generate a modulation on the RF drive signal to the TWLA. Several features make this attractive.

1. The need for a high quality frequency signal generator is eliminated. The signal rate is "self adjusted" to the cavity length, thereby eliminating the need for closed loop cavity adjustment for dimensional drift.

2. Extremely short electrical control pulses can be "self-generated" by this method *if* the laser gain medium, the detector, and the amplifiers have sufficiently high bandwidth response, *and if* the amplifying chain can deliver sufficient electrical power, *at these frequencies*, to achieve sufficient modulation.

Although the optical signals are self referencing, electrical filtering is required to select the desired harmonic, and an RF delay line (phase shifter) is required to synchronize the opto-electronic feedback signal with the optical pulse train in the cavity.
The main reason for modelocking this type of system by the two complementary methods was to compare their stability and noise characteristics in systems that are otherwise as identical as possible. Investigation of pulse widths was done to determine the extent to which the results were consistent with theoretical models.

Experimental Results

It was found that the saturation output of the high bandwidth electrical amplifiers (about -20 dBm) was insufficient to provide the required modulation depth for modelocking at the current threshold levels for this device. An additional stage of high power amplification was therefore added to bring the feedback signal up to +20 dBm. This however limited the final stage bandwidth, and hence the system as well to a value of about 1 GHz. The data on the resulting pulse train (fig. 18) again shows freedom from satellite pulses with primary pulse durations approximately the same as the actively driven ones. Although in theory they could be as short as the transform of the gain bandwidth (100 fsec), the final output pulse width will in fact be limited by the slowest responding element in the chain. We note that a duration corresponding to the transform of a 1 GHz electrical limit is consistent with the measured result broadening to 50 ps.

Timing Stability and Noise Analysis

Since both types of pulse trains had similar width, a fair comparison of frequency noise could be made.(fig. 20,21) It is apparent that the active modulation is free of measurable frequency noise within the resolution of the spectrum analyzer (HP 8701). The regenerative data however reveals effects of both broadening and an increased noise floor. A quantitative analysis can be performed on the frequency spectrum data enabling an estimation of both the pulse to pulse amplitude and temporal variance[11]. It can be shown that with the use of some reasonable approximations, that the pulse's temporal variance Δt and the pulse amplitude variance ΔE are given by the following expressions, involving integrated noise measurements that can be performed with a high resolution microwave spectrum analyzer.

$$\left(\frac{\Delta t}{t}\right)^2 = \frac{S_n - S_1}{P_n(\Delta \nu)}$$

$$\left(\frac{\Delta E}{E}\right)^2 = \frac{S_1}{P_1(\Delta \nu)}$$

TEMPORAL and AMPLITUDE VARIANCE (Δt, ΔE)
[extracted from integrated noise measurements in the microwave domain]

where S_1 = integrated noise in first harmonic order
and S_{an} = integrated noise in the n th. harmonic order
(The 8 th harmonic was used here)
t = pulse width E = pulse energy
Δt = temporal variance(jitter) ΔE = pulse amplitude variance
$\Delta \upsilon$ = spectrum analyzer resolution bandwidth
P_n = power in the "**n**" th harmonic

Analysis of Timing Jitter Comparison

The results of the previous analysis are extremely useful. The pulse's energy (amplitude squared) variance is given by the noise spectrum in the fundamental order, whereas the temporal fluctuation (timing jitter) can be found from a higher order noise integration. The model in fact predicts timing jitter noise to increase precisely as the square of the order number, while the amplitude noise does not change at all with the order. In practice one takes the highest harmonic of the fundamental frequency allowed by the bandwidth of the spectrum analyzer. The data taken at first and eighth harmonics by the two mode-locking methods is given in figures 20,21. A comparison shows that the active mode-locking has very little difference between orders, indicating extremely low timing jitter. The amplitude noise from eqn. 5 is found to be about .0004% or about 0.2 ps (as an upper limit). The regenerative method however, shows not only a much higher amplitude noise figure, but also an increase in the high order noise, which is indicative of timing jitter. The magnitude given by eqn. 7 is about 0.2% which corresponds to 3 ps at this repetition rate. Though this is significantly higher than the sub-picosecond active modelocking instability, it should be emphasized that this is still less than most other methods of generating short pulses at this wavelength. For example, gain switched diodes and modelocked flashlamp pumped Nd (YAG or YLF) systems typically display 5 to10 picosecond timing jitter. The modelocked 1319 nm Quantronix YAG used for in-house TDM experiments has been measured at about 8 picosecond temporal variance. This value is in fact of critical importance and acts as a limiting factor on maximum data rates attainable with a given source. To a first order approximation:

$$\text{Max TDM rate} = \text{Period}/[(\text{Timing Jitter}) + (\text{Pulse width})]$$

It is apparent from the summed dependence in the denominator that no matter how short the pulse is, its pulse-to-pulse temporal stability is of greater significance for any TDM type applications, whenever the variance is on the order of (or greater) the pulse width.

To illustrate this with actual sources:

	Pulse Width	Timing Jitter	Max TDM rate
Pulse compressed Quantronix YAG	1.5 psec	8 psec	100 Gbits/sec
Regeneratively modelocked TWLA	48 psec	0.6 psec	20 Gbits/sec

(Note that in the first case the rate limitation is dominated by the jitter, while in the other it is mainly determined by the pulse width.) The general observation to be drawn is that to achieve data rates in actual practice on the order of 1 Tera Bit/sec, **both** pulse width and timing jitter must be on the order of one picosecond or less.

Sources of Timing Instablity

Several noise mechanisms contribute to the results found here, besides those anticipated from only the detection and amplification stages. In this particular gain medium the carrier density is directly modulated, not the amplitude itself. In the second method

where the cavity mode itself is amplified, the carrier density also modulates the path length (via the optical index of refraction). The *time-bandwidth product* resulting from this data (approximately 12) confirms the fact that the pulses are far enough from the transform limit to ignore the effects in this application. The transform limited case would be about 0.3 for the time bandwidth product. Theory is detailed in section 5.

Performance Data Summary

CW Power	0.5 mW
Pulsed Power	1.0 pico Joule
Pulse Duration	40 pico seconds
Bit Rate Limit	12 giga bits

Stability Analysis

	Actively Driven	Regenerative (Passive)
Amplitude	--	1 %
Temporal	--	8 pico-seconds

Conclusions

A TWLA chip was successfully incorporated as the gain medium in a diode based laser signal source system. Constructing an external cavity wavelength tunable diode laser was readily achieved. This is of great useful interest in itself since the diodes themselves are convenient, relatively inexpensive, and are available at nearly every wavelength of practical interest. Wavelength tuning is needed in many different kinds of applications. Subsequently, commercial versions of CW tunable diode lasers have surfaced in high price ranges (50 k). Only more recently (1994) has the price come down to the 10k region in the relatively simpler CW versions.

The majority of applications, however, require pulsed operation. For this, theoretical models were assessed (fig.19), and detailed quantitative temporal stability measurements were performed and analyzed. At the time this was, to our knowledge, the first time this was done. The summary of what was learned emphasizes applications as well as the experience gained in laser design and construction. Active modelocking has superior stability, but passive types can produce shorter pulses, even at lower repetition rates. In this work described, a well understood electrical response prevented the regenerative passive method from attaining the theoretical limit of time bandwidth product. From the experimental observations given here, it can be inferred that future advances enabling terabit rates will require the short pulses from appropriate passive modelocking mechanisms to be combined **in the same system** with active control for superior temporal stability. This has come to be termed "hybrid" modelocking. In a sense this experimental work may have been one of the first studies of these complementary features in the same system. The next step would have been combining the desirable features in a hybrid scheme. This in fact was accomplished much later but in a

completely different system based on a fiber laser. The principles learned from this work, however, have remained valid and in fact guided the development of more recent follow-on work. Similar system work was pursued by Peter Delfyett at Bellcore in the 800 nm regime. This approach produced an innovative successful method of "seeding" a regenerative amplifier with an external cavity diode laser in place of a massive Argon/Ti-Sapphire combination. He is now extending this to 1.3/1.5μm systems on a contract from Rome Laboratory in his new location at CREOL in central Florida.

Acknowledgments: J. Lacourse and R. Boudreau @ GTE Laboratories for providing active waveguides and P. Delfyett @Bellcore for helpful discussions of cavity configurations.

4.0 TIME BANDWIDTH PRODUCT ANALYSIS

A significant portion of papers involving very short pulses include a measure of the spectral spread, generally given as a half power band width (HPBW), as well as the temporal half width of the pulse itself. In practice, the optical frequency bandwidth is calculated directly from the optical spectral data in wavelength. The product of the temporal and frequency half bandwidths is then cited as the Time -Bandwidth Product. The actual significance of this analysis is generally glossed over and often only the final results assumed. It is worth deriving the key results in some detail, not only to clarify it for some of those working in this field, but also because the results can easily be misinterpreted. The content of this section was prompted by the need to determine if modelocked pulses in several of our lab experiments involving solid state and fiber lasers were transform limited.. This provides essential information regarding frequency chirp content of the pulses as well as dispersion in the media.. This is presented in some detail, including sample calculations, because no available references explain the terminology, procedures, or the significance in a clear consistent manner. This may then serve as a useful reference.

The general significance derives from the fact that *time* and *frequency* are Fourier conjugate parameters. In the derivation of modelocked laser pulse profiles, which we need not reproduce here, it can be shown directly that a uniform phase separation between the modes leads to a Fourier Transform relationship between time and frequency **amplitude** profiles. This applies rigorously to the generally realistic case of inhomogeneously broadened media. Such pulses are referred to as **transform limited** since the profile in time is precisely the transform of the frequency profile. If the phase relation is however not uniform between the modes, then the resulting pulses are denoted as being chirped and a rigorous theoretical calculation shows that the resulting pulse widths must be wider than transform limited. The importance in laser cavity design and diagnostics is derived from the fact that one can determine if the pulses are as short as possible, and whether there are dispersive or other mechanisms present in the laser medium, which may warrant optimization.

For the case of transform limited pulses, the F.T. dictates a direct relation between the frequency spread necessary to constitute a given temporal pulse width. An immediate straightforward result is that a very short pulse requires a wide frequency spread, and conversely , a very narrow spectral output $\Delta\lambda$ from a laser is possible only over a large time interval Δt. Hence ultra narrow line lasers are nearly always CW, and very short pulsed lasers require a large spectral emission bandwidth. Such results are apparent upon taking the Fourier transform of various functions f(t) resembling real pulse shapes and noting the widths of the transforms F(ν). This reasoning applies equally in the reverse order starting from the spectral data trace and extracting the projected pulse shape.

At this point the conventional form of the time bandwidth product is defined as:

Definition : TBWP $\equiv (\Delta t)(\Delta \nu)$

Here Δt and $\Delta \nu$ are both halfwidths of the **intensity** (or energy density) profiles, which are in turn proportional to the squares of the amplitude profiles. The reason for this is simply that the intensity (proportional to power) is the parameter actually measured by test equipment based on normal detectors. It must be emphasized however that the Fourier Transform relation applies here to the amplitude (or **E** field) profiles, not the measured intensity ($\mathbf{E}^2$). These two functional profiles are in general quite different. When the measured TBW product matches that of the calculated transform width relation, then the pulses are transform limited. Among others, this indicates the shortest possible pulse.

Measurement Considerations

Some clarification is useful regarding what is measured. The temporal profile can in principle be measured by an oscilloscope, if the impulse response time is sufficiently faster than the pulse width. For pico and femto second pulses this is speed not sufficient and an autocorrelator is used. Pulse shape extraction cannot in general be done directly without assumptions, and then only with the appropriate form of deconvolution (ref.) The frequency width is generally calculated from the measured optical spectral width by the standard differential relation in terms of υ(frequency) and λ(wavelength).

$$\Delta \nu \cong \frac{c \cdot \Delta \lambda}{\lambda^2}$$

Let us take a common and realistic pulse shape as:

The temporal amplitude is $\mathbf{f(t) = \exp(-\pi t^2)}$ **i.e. Gaussian.**
(Proportionality constants have no effect on these results and will be omitted throughout.)

The intensity or measured profile is $\mathbf{f^2(t) = exp(-2\pi t^2)}$
which in this particular case is also a Gaussian, but a different one than the amplitude.

The amplitude Fourier Transform is $\mathbf{(\nu) = exp(-\pi \nu^2)}$

and the corresponding intensity is $\mathbf{F^2(\nu) = exp(-2\pi \nu^2)}$

In this case there is complete symmetry because the Gaussian function happens to be its own Fourier transform. This is true of a few common functions.
Since complete functional shapes are not always straightforward to extract directly from measurements, the half power bandwidth is often used because it is simple to measure. For this reason the TBW product is defined as the product of the HPBW of the intensity functions in time and frequency. This quantity can now be easily calculated in this case.

Referring to the sketch of a Gaussian on next page, centered at t=0;
and letting Δt=HPBW

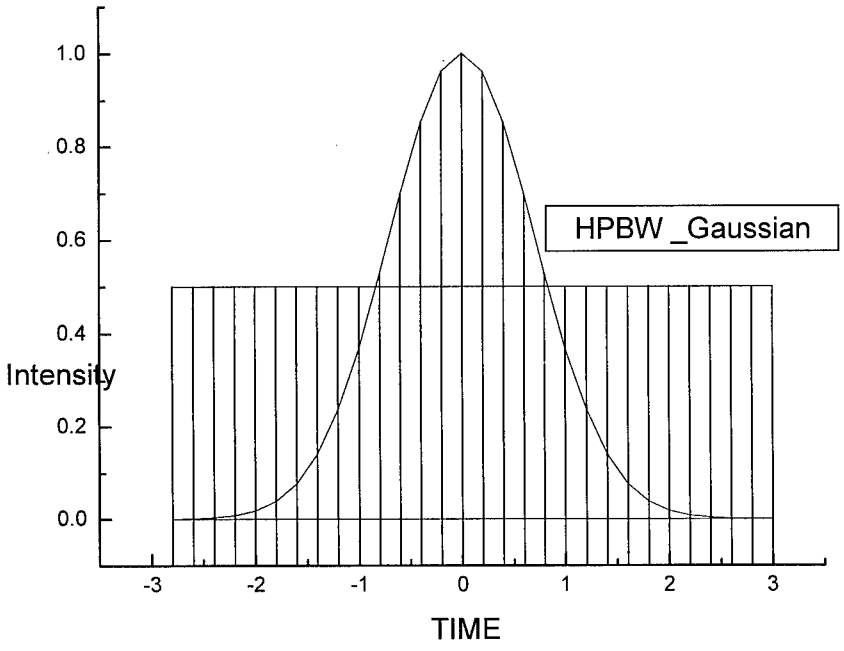

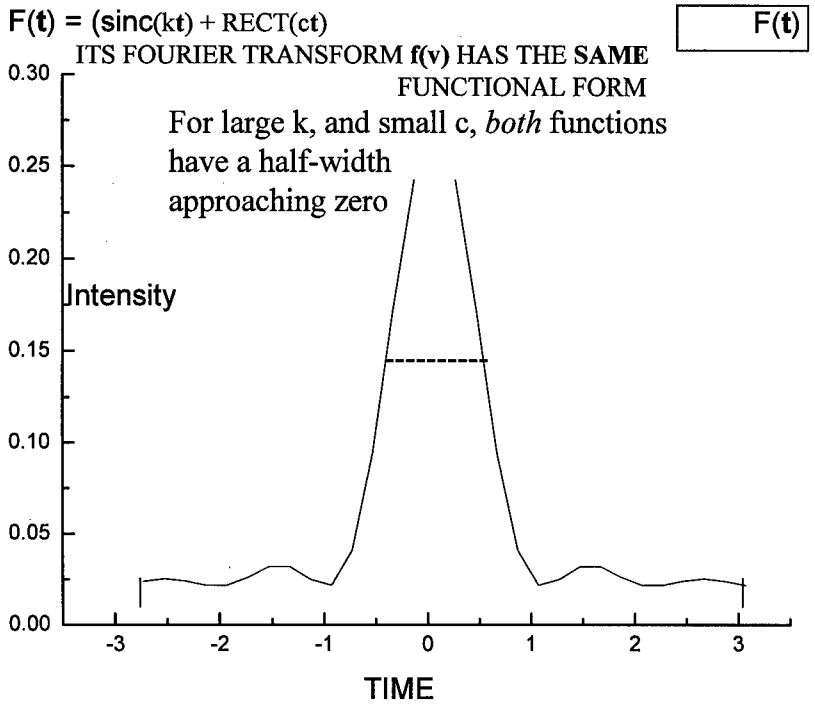

One can then solve:

$$\exp(-2\pi T^2) = 1/2 \quad \Rightarrow \quad 2T = \Delta t = \sqrt{\frac{2(\ln 2)}{\pi}}$$

The squared Fourier amplitude transform in units of frequency [where $\nu=1/t$] is of identical form as the time calculation so the HPBW in frequency is also:

$$\Delta \nu = \sqrt{\frac{2\,(\ln 2)}{\pi}}$$

Therefore: **Gaussian TBW product $(\Delta t)(\Delta \nu) = 0.44$**

There is a standard and commonly cited reference, which lists several of the common shape results(3). It is however not very clear on the definitions or assumptions for such data analysis, and even contains some errors on certain pulse shapes.
If one knew somehow that the pulse and frequency spectral shapes for a given measurement were Gaussian, and if the TBW product yielded 0.44, this would then indicate what is termed *transform limited performance*.

The more prevalent shape for many types of modelocked lasers and solution based pulses in particular, is the hyperbolic secant. In the intensity format it would be **$\mathbf{sech^2(\pi t)}$**
The factor of pi is included to maintain symmetry under transform, since sech(πt) is also its own Fourier transform. By symmetry we again need only one width calculation to find the TBW product. The calculation is done by solving the simple transcendental equation:

$$\frac{2}{\exp(\pi T)+\exp(-\pi T)} = \frac{1}{\sqrt{2}}$$

The result is: $2\,T = \Delta t = \mathbf{0.56}$ So $\Delta\nu = \mathbf{0.56}$ as well

and so the **Sech(t) TBW product = 0.314 = $(.56)^2$**
This function is most important in fiber laser and solution pulses. In the sections giving actual experimental fiber laser data analysis presented later, this product condition is quite precisely satisfied in several real experiments.

A **Lorentzian** pulse shape on the other hand is not its own Fourier transform. (It is in fact the **exponential function.**) The TBW product is still found from similar calculations as:

Lorentzian TBW Product = 0.210 which is less than either of the previous.

A few questions present themselves.
1) Can one get useful information from the TBW product alone without full pulse shape knowledge?
2) Is there a lower limit to the TBWP? If so, what is it?

The motivation for the second question is the well established fact that the Gaussian function and its self-transform constitute a minimum of all functions for "time bandwidth uncertainty product." It must be emphasized that this applies **only** when the "uncertainty spread" is defined as an **RMS width** rather than a half power width. This forms the basis of a well known theorem in Fourier Transforms, as well as a representation of the Heisenberg Uncertainty Principle applied to wave packets.

Before discussing the RMS definition, question 2 will be answered by showing that in fact the TBWP defined by the half-power has **no lower limit**. This is seen directly by conceptually taking a non physical function composed of the sum of a constant and a delta function. The linearity of the FT means that the FT of the sum is the sum of the F.T.s. This procedure yields again the sum of a delta function and a constant. The half width of both squared versions approaches zero as a limit, so the TBW product is zero. This calculation can also be done rigorously with real physical functions, as is illustrated in fig 4a with a very wide Rect(ct) and a narrow Sinc(kt). Each functional sum again transforms into the other, and both can be seen to approach zero width. The resulting

TBW product then clearly must approach zero as well. It will be seen that this somewhat disturbing result is not the case for the RMS approach.

The RMS Method for Time Bandwidth Product

$$\text{RMS\_width} = \frac{\int_{-\infty}^{\infty} t^2 \psi^2(t)dt}{\int_{-\infty}^{\infty} \psi^2(t)dt} \qquad \text{Let } FT[\psi(t)] = f(\nu)$$

The definition: $(\Delta t)(\Delta \nu)$ = TBWP applies to RMS as well.

Gaussian: Let $\psi(t) = \exp(-\pi t^2)$ $F.T(\psi) = f(\nu)$ has the same form so $\Delta\nu = \Delta t$ RMS.

$(\Delta t)^2 = 1/4\pi = .0795 = (\Delta t)(\Delta \nu)$ **(Gaussian RMS)**

Note that this value is approximately the square of the half power version as would be expected, since the "average" value of t^2 was effectively calculated in the RMS case. It is interesting to compare this result with that of the Sech(t) function, which turns out to apply to many nonlinearly generated profiles in solution pulses. The result is given without further detail.

$(\Delta t)^2 = 1/12 = .0833 = (\Delta \nu)(\Delta t)$ **(Hyperbolic secant RMS)**

A proof due to W. Pauli shows that a Gaussian yields the minimum value of this (RMS) product obtainable by **any** function. Interestingly the sech function's value is close but greater, by the half power version given in the previous section, this was reversed. The reason for this behavior is clearly due to the fact that half width method does not "integrate" the lower base contribution, while the RMS approach computes a full weighted average due to the contributions from the **entire function**.

It would certainly seem that RMS should be the proper and universal way of defining TBWP. The answer is probably the affirmative, but it requires extensive data and computation as opposed to a single measured value. However, data acquisition is becoming more automated along with computational capability, so a change may in fact be facilitated in the reasonably near future. In the meantime there is still some value to the traditional half power definition.

Conclusion

The real drawback of the half power approach is the unavoidable ambiguity. Even if the measured TBW product corresponded to the theoretical value for a given profile; the information is not meaningful without assuming (or confirming by measurement) the exact functional shape. In particular, the presence of a chirp can broaden a pulse so that the TBWP for a given profile can yield the same exact value as the transform limited

product of a different profile. This obviously defeats the main point of such analysis. This is not explicate acknowledged in most journal literature. Even with such an awareness, it is commonly *assumed* that the pulse shape corresponds to some theoretical model for that laser, and that the data therefore conforms reasonably to that profile. The crucial point is that the RMS approach has no need for any profile shape assumptions whatsoever; they are supplied by the actual measured data. Therefore, if one has enough data to justify a profile, there should be enough to enter it in the RMS analysis. Rigorous TBW values are then generated with *no assumptions*. With advances in the data acquisition, such analysis can be incorporated in some future Rome Laboratory papers on the modelocked erbium fiber lasers and also the solid state chromium doped YAG laser. It is anticipated that this would stimulate and support future trends in this direction at other locations as well.

5.0 RAMAN SHIFT TO 1.55 μm

A previous project was done involving Raman shifting of 1.06 μm light to a wavelength of 1.55 μm, (fig.22) which is both eye safe and in the region of prime fiber optic interest. The initial set of experiments for this was performed and documented as one of the three sections of the LDF technical report on nonlinear optics which I completed in 93. I will not include here any of that work except to describe subsequent follow on work, which was assimilated under P207. A brief review is needed, however, to provide a proper perspective. The Raman primary Stokes shift in Deuterium (1057 cm^{-1}) is extremely large. This downshift in frequency (up shift in wavelength) holds even when suspended in media such as glass, optical fiber, or liquid ethanol in particular.
The technology used to "dope" deuterium into a fiber core, by extended exposure to high gas pressure, was the forerunner of the present method of "loading " hydrogen in doped silica fiber core. This is now an established method of sensitizing optical fiber for UV writing of Bragg fiber gratings. In liquid ethanol, when hydrogen atoms are replaced by deuterium atoms, the transparency region becomes extended from about 900 nm to well beyond 1.55 μm. Samples were obtained from a chemical supplier, and a set of in-house experiments determined that a focused beam from a Q switched YAG laser could achieve over 5 % conversion efficiency from 1.06 to 1.55 μm. The key point is that convenient sources providing short pulse and high power are not available at 1.5 μm.

Raman Efficiency

The Raman effect is non- resonant and so works at all wavelengths in the range of transparency. The quantum efficiency, however, *decreases* as the square of the wavelength. The significant limiting mechanisms were identified by theory and confirmed in the initial experiments. The efficiency is peak power dependent, while the laser damage threshold is energy dependent. The weakest point for optical power damage is at the index discontinuities on the window interfaces where the E field differential is greatest. This problem would be mitigated by high quality AR coatings, which were subsequently obtained . It was also observed that the beam divergence induced by the

Raman scatter required field lenses for practical free space propagation. This poses problems for application as a compact laser radar accessory, but not for our prime emphasis as a source for fiber optic applications and diagnostics. Most of the latter ultimately require pulses much shorter than the Q switch limit of about 10 ns. The ideal source for this is a Q switched modelocked YAG laser.

Ultrafast Conversion

A Ti Sapphire laser, installed at Rome lab, provided an opportunity for generating femto second range pulses. This permits testing the conversion efficiency under the nearly ideal conditions of very high peak power with moderate energy, a natural combination for very short pulses. The wavelength would initially be centered at 810 nm rather than 1.06μm, but the principle would be one of very general interest and utility, particularly since many other solid state lasers, existing or under development, would be able to use this method of converting to longer wavelengths when required.

Power Requirements - Regenerative Amplification

The power needed for this experiment turned out to require a regenerative amplifier accessory to the Ti_2O_3 laser, which was not installed on our system. However the manufacturer of the system, Clark MXR, (fig.23) offered to let the experiment be done on their system. The pulse width was about 120 femto seconds centered at 810 nm with a pulse energy of 1 millijoule at a kHz rate. The configuration and parts required as shown in Fig 6 were fairly straightforward. After some normal problems of lining up optics, sample cells and adjusting wavelength the results came out negative (no conversion) for the deuterated ethanol. To rule out the possibility that sample degradation or contamination of the d_2-alcohol compound had affected this result, a control sample of acetone was also tested. The latter has slightly less crossection, and poor transparency at 1.55 μm, but this does not impair this particular test. The result was also negative. The theoretical effect working against this process was the fact that in the pico second and sub pico sec regimes, the Raman effect (which is a molecular energy transition) becomes transient. This means that its response time cannot absorb the full power of a substantially shorter pulse. No quantitative theory or experimental data was available regarding Raman conversion in these materials, so the best choice was to perform the new experiment.

Conclusions

The Conclusion is fairly definite: the extremely high peak power available from an amplified fsec range laser, is insufficient to overcome the loss effects from very low temporal overlap in the transient regime. Ideally one would perform a more complete set of temporal width selections. If one worked back from the 10 ns (Q-switch) regime, where it works, one could establish the transient threshold level and efficiency. Unfortunately this effort would not be justified since our main interest is the actual

conversion of very short rather than intermediate range pulses. Subsequent literature searches have found some success in this type of conversion at a laboratory in Germany. The wavelength was however in the ultra-violet, where the previously mentioned wavelength dependent quantum efficiency predicts more than an order of magnitude advantage in threshold level and conversion efficiency. Since the prime interest here was in the practical application at key wavelengths of interest, and not in the interesting physics for its own sake, the project was considered concluded. The Q switched conversion, which was moderately successful, did provide some useful laboratory tools but no likely field applications. Even though the ultra short pulse result was not successful, it still justified the effort to explore and extend the use of in-house equipment for a new and useful purpose. The need for versatile sources at 1.5 μm is being pursed by other methods such as solid state lasers doped with erbium doped glass and modelocked types based on chromium doped YAG crystals.

6.0 FIBER AMPLIFIERS

The availability of rare earth doped fiber made it a natural medium for fiber based devices. Several reported characteristics indicated significant advantages over other optical amplifiers. Since this application was being extensively explored by the doped fiber vendors themselves as the fiber was being developed, we had no need to duplicate their work. In particular AT&T, Corning, GTE labs, Fujukara, and Lycom, competed in fiber and amplifiers. The main thrust was, of course, erbium doped fused silica fiber for use at 1.5 μm. Other ones were Neodymium doped silica fiber for use at 106 μm. 1.3μm posed a problem in that Neodymium doped silica which would be the natural choice with a strong emission band there was ineffective due to extreme excited state absorption.

Some limited tests of amplifier performance were done in our laboratory to be certain that the characteristics were understood and could be exploited for various applications in signal processing. It was also clear at this time that the potential for a fiber based laser was a possible unique opportunity for Rome Laboratory, which could not be properly pursued by the fiber development vendors themselves because of their limited experience in high speed signal processing.

Erbium Doped Silica Fiber

Erbium/silica fiber demonstrated a fortuitously remarkable combination of properties making it highly suitable as a gain medium for optical amplification.

1. Long upper state lifetime
2. No excited state absorption
3. High gain /conversion efficiency
4. High saturation output power-- proportional to pump power
5. Emission wavelength centered at the low loss region of fiber signal propagation
6. A broad fluorescence spectrum capable of sustaining ultra short pulses

7. Excellent physical mechanical properties

The first property cited is ironically the one which provides a decisive advantage over diode based amplifiers. Due to the very long upper state lifetime (several milliseconds) the gain remains essentially constant for signals in the pico-second regime. Thus the intersymbol **gain recovery** variance noted in diode based amplifiers is avoided when the pumping level is sufficient to approach saturation. The distinction between this property and the amplifier response time must be emphasized. Each single pico-second width pulse is amplified without temporal distortion, since the **response time** of the erbium gain medium is in the femto-second range. This time constant is governed by the fundamental emission/absorption line width, which is sufficiently broad spectrally (40 nm) to sustain femto-second pulse structure. Erbium doped fiber thus possesses most of the properties required for applications and fortuitously operates at the wavelength of minimum fiber propagation loss. Future fiber based systems will definitely emphasize the 1.5μm fiber window because of these factors.

Neodymium Doped Fiber

The tests showed one characteristic which was actually slightly advantageous over erbium. Neodymium operates as a four level laser (erbium is three level above cryogenic temperatures). This means its ground level is not directly involved in the lasing transition, so that it remains transparent to the signal in unpumped regions of the fiber. In a three level system, the unpumped doped medium becomes an attenuator/ absorber. This makes length/pump power matching critical in erbium fiber and relatively non critical in neodymium. The gain is lower in neodymium and of course the wavelength is not useful in most fiber optic signal processing. It is useful for chirp effects in Yag laser pulse compression systems. Livermore and the Laser Energetics Laboratory at Rochester actually utilize such fiber in some versions of the "Seed Laser" which generates a perfect pulse shape for subsequent amplification. This is of course not strictly in the signal processing region of prime interest at Rome Laboratory.

Praesedymium Doped Fluoride Fiber

This fiber provided the only viable alternative in the still important fiber window at 1.3 μm. It possessed the first 6 of the desirable properties though gain and conversion efficiency were significantly lower than erbium. The disastrous shortcoming is in the seventh category. The proper emission for praesedymium can be achieved only in a fluoride based fiber. The mechanical properties are extremely poor. Cleaving is unreliable and fusing is next to impossible. The price is also an order of magnitude higher than erbium fiber. The experience gained in setting up this amplifier confirmed that this was not likely to be useful for most practical applications. Even in recent times, only one commercial vendor (Hewlett Packard) has attempted a product based on this. It is of course fitted with bulkhead connectors so that no user ever needs to access any fiber directly. The two methods used for our in-house measurements were:

1. Careful hand cleaving of the fiber ends, with index matched butt coupling guided by V-Grooves.

2. For comparison, one length was sent out for special connectorization. This is of course the ideal procedure for unmanageable media, since almost any material can be polished when properly mounted and supported. Some of this is occasionally done in house, but for FC/PC compatibility a special set of curved polishing fixtures is required.

The performance of the two methods is similar. Changing the fiber length by cutting back is however, a fairly cumbersome procedure for either of these two methods. When it became necessary to change the length by cutting back fiber, clearly the second method is so time consuming as to preclude this . This is in contrast to the simplicity of an automated cleave and fusion splice, which is routine with most erbium doped fibers.

From fig. 12 the fluorescence region is seen to be well located for 1.3μm application, and is also wide enough to sustain short pulses. However comparison with fig 13 shows how much lower the emission level is compared with a length of erbium doped fiber. It should be noted these were not identical lengths or dopant concentrations. In general, a shorter length requires more pump power to achieve optimum gain. This poses a dual problem. The fiber cost makes long length very expensive. Furthermore, obtaining high pump power is not straight forward at the main absorption band centered at 1.017μ. This is even further down the gain curve of the Ti sapphire laser than 980 nm. The net result is about 100 mW available prior to fiber launch. At that level it is preferable to use a MQW fiber pigtailed diode laser delivering 50 mW peaked at 1.017μ. This is what was actually done.

Co-Doped Fiber

It is possible to place more than one dopant into the fiber core in order to combine desirable properties. One of the most useful is the erbium/ytterbium combination. It has the very useful property of shifting the absorption peak toward 1.06 μ, thereby permitting a high powered neodymium based pump laser. This type of fiber was not obtained for this project because of the practical emphasis on compact diode laser pumping. It would be the fiber of choice for very high power applications such as free space laser eye-safe radar.

Mode Matching

Optical fiber provides a unique low loss conduit for high bandwidth signals. The main losses come from coupling into the small area core (8 μm dia for std fiber). This is even more important in erbium doped fiber with typical core dia <4 μm. What actually counts is the mode field diameter, which can be calculated from the particular fiber index profile design and dimensions. We need not go into these details, but it is important to be aware

that coupling between any two different fibers entails a calculable loss in at least one direction of propagation if the connection is a straight butt coupling.. This can be approximated by visualizing the area of the smaller core overlaid on the larger. The evolution of erbium (and other rare earth doped) fiber has shown advantage in gain by use of smaller cores providing more uniform confinement of the overlap with the dopant population density. Thus a very small core must be coupled to normal telecom fiber several times in nearly all amplifier / laser systems.

Conclusions

Based on the extremely desirable characteristics of Erbium doped fiber, several fiber amplifiers were constructed and versions of them are still in use. The other doped fibers were of some theoretical interest, and resulted in thesis work, but were not considered to be of great practical interest to the future project work. It was decided to utilize the successful erbium based technology in the development of modelocked fiber lasers for signal processing applications. This is described in the following sections.

7.0 ERBIUM DOPED MODELOCKED FIBER LASERS

The fiber laser project evolved from the work initiated in optical amplification and fiber amplification in particular. My involvement in this work was included in this project number for the past year, and much of it has been pursued in conjunction with Professor Teegarden. Unlike some other projects, this one has been well summarized in numerous papers for conference presentations. To avoid unnecessary repetition, I have included relevant contents from a selection of those on which I was the primary author. These describe the two successful types of modelocked erbium lasers which have been developed at Rome Laboratory. The first is based on a fiber ring laser and the second is a standing wave cavity. The latter one is in the process of patent preparation.

7.1 Kerr Effect Passively Modelocked Erbium Doped Fiber Laser (System #1)

We report the development of a simple self starting passively mode locked diode pumped laser oscillator utilizing erbium doped fiber (fig.24) and a minimum number of standard components. With pump powers as low as 8.0 mW, the fiber laser generates stable pulses of 1.2 ns width and rates of 5.0 MHz at wavelengths near 1.55 μm. At higher pump power pulses from 10 to 35 ps are observed. A mechanism for the observed characteristics of this laser based on the optical Kerr effect is proposed.

INTRODUCTION

Various types of mode locked fiber lasers have been developed [1,2] to produce short pulses at wavelengths in the 1.55 micron telecommunications window. Such lasers are attractive sources of pulsed signals or optical solutions and are therefore important in advanced broad band optical communications systems where very short pulses are needed. Most

mode locked fiber lasers developed to date can produce pico-second or sub-picosecond pulse widths only with the use of fairly complex cavity designs. These laser designs in general require high pump powers and critical alignment conditions to be met.

OBJECTIVE

The objective of the present work was the development and characterization of a portable alignment-free laser, based largely on commercially available components. In particular, the conversion of a commercial erbium doped fiber amplifier to a mode locked laser was experimentally investigated. In this report we describe a simple self-starting diode pumped mode locked laser involving a minimum number of components.

EXPERIMENTAL RESULTS

The layout of the ring laser is shown in figure 24. An erbium doped fiber amplifier was used in a unidirectional ring laser configuration. The output of the fiber amplifier was connected to its input with standard fiber couplers, a polarization controller, and a pigtailed isolator of the Faraday rotator type. These components were fusion spliced together to minimize reflection effects which reduce the bandwidth available for modelocking. Both in-house and commercial optical amplifiers were used as the gain medium of the ring laser. The in-house amplifiers consisted of a length of erbium doped fiber pumped with a 100 mW diode laser operating at 980 nm (Spectra Diode Laboratory's SDL-6312-HI). A fiber wavelength division multiplexer (WDM) was used to mix the pump radiation with the circulated 1.55 nm output. The diode laser output was collimated with a 20x microscope objective and focused onto the input fiber of the WDM with a 5x objective. This launch system resulted in about 45 mW of pump power at the output of the WDM. A significant loss in pump power occurred at the splice between the WDM output and the erbium doped fiber due to the mismatch in fiber diameters at this point. The diameter of the core of the fiber at the output of the WDM was 8.0 nm while the doped fiber core diameter was ~5.0 μm. The measured loss due to mode mismatch at this point was about 1.25 dB.

Some of the problems described above were eliminated by the use of a commercial fiber amplifier (Corning Fiber Gain Module model P3-35). In this case a pigtailed pump laser operating at 980 nm, the WDM and doped fiber were all included in the module. These components were integrated in the amplifier design to provide stable high gain at minimum pump powers. Similar results were obtained using amplifiers constructed in house based on erbium doped fiber supplied by GTE Laboratory or Brown University.

The rest of the ring cavity was constructed from readily available components including standard single mode telecommunications with minimum dispersion at a wavelength of 1.3 μm, so the cavity was in the anomalous dispersion region at 1.55 μm. Several different splitting ratios between the output signal and the feedback signal were tried. In the case of the high gain commercial amplifier, a ratio of 50/50 gave the maximum output

power. The in-house amplifiers had a lower gain and required a 90/10 feedback ratio to optimize the power.

The isolator and polarization controller were essential to stable operation of the mode locked performance. Two types of pigtail Faraday isolators were used. The first was non polarizing (OFR IO-G-IR2), the second included a polarizer and therefore acted as a polarizing element(OFR IO-G-IR2). The fact that no significant performance difference was observed, is still puzzling in view of the theoretical analysis given in the last section.

Both the optical spectrum and the temporal characteristics of the output of the oscillators was examined. Spectra were obtained with a commercial optical spectrum analyzer (Anritsu MS9OOlBI). The temporal characteristics were observed using either a fast photodiode amplifier combination (Lasertron QRX-700) and a digitizing signal analyzer (Tektronix DSA 602) or an avalanche photodiode (Antel AMF-20, Mod. MARG-20) in combination with a digitizing sampling oscilloscope (Tektronix 11801). The first combination featured high sensitivity and rapid response but had a band pass of 500 MHz. The band pass of the second combination was measured to be 7.54 GHz corresponding to a resolution of 133 ps. In addition to these instruments, an optical autocorrelator (INRAD 5-14-AD) was used to detect structure faster than the resolution of the above detection systems.

DATA ANALYSIS

The optical spectrum and the temporal behavior of the laser output were examined as a function of pump power. It was found that at threshold and above, the output always consisted of a CW component and a periodic series of short pulses. No special effort was needed to initiate the short pulse component. The period of the pulses was stable and independent of pump power. An oscilloscope trace obtained in this way, near the threshold for lasing action, is shown in figure25. In this case the period of the pulses was 189.2 ns, corresponding to a frequency of 5.285 MHz. The average pulse width was measured using a detection system with a band width of 7.55 GHz., and found to be 1.246 ns.

The time averaged output of the oscillator was measured as a function of launched pump power using a standard power meter. The launched pump power at threshold was found to be about 4 mW. while the output power was 3 mW for a pump power of 25 mW.

The optical spectrum of the oscillator was also measured as a function of pump power. Near threshold the spectrum consisted of a band with a full width at half maximum of about 2 nm. centered at 1.556 nm. As the pump power was increased, oscillation occurred in several narrower bands as is illustrated in Fig. 5. The central band had a half width of about 0.5 nm.

The temporal behavior of the oscillator output was also measured with an autocorrelator. The presence of temporal pulses with a full width at half maximum of about 35 ps. was

indicated by this data. However at pump powers near threshold the output power of the laser was too low for autocorrelation measurements to be made.

THEORETICAL ANALYSIS

The appearance of a stable train of short pulses with a period set by the length of the cavity indicates that self mode locking was occurring in the laser cavity. This is supported by the presence of structure on a picosecond scale in addition to broader nanosecond pulses. The broad spectral band observed near threshold indicates the possibility of some bandwidth limited structure as narrow as 2 ps.

NONLINEAR KERR EFFECT -- POLARIZATION EVOLUTION

The probable mechanism for the observed passive self-modelocking in the fiber ring laser is a nonlinear polarization evolution. This is somewhat analogous to the Kerr lens self mode locking that has recently revolutionized femtosecond pulse generation in solid state Ti:sapphire lasers. While spatial lensing does not occur in single mode fiber, certain other effects, such as those which are utilized by the usual optical Kerr gate, can apply to fibers. The single propagating mode in an optical fiber is degenerate and supports two orthogonally polarized eigenmodes. Thus if a high intensity "pump" flux (in one polarization here chosen as "x") alters one of the refractive indices, the result is a relative phase change for any propagating signal which has components along both polarization axes. This phase change is intensity dependent with a magnitude determined by the field strength of the pump beam and by the relevant nonlinear coefficient. If one visualizes a linearly polarized signal beam launched so as to have equal components in both axes, i.e., $\theta = 45°$ from the pump polarization axis, it is clear that any relative phase change induced by the pump beam will result in elliptical polarization. A component is therefore generated which is orthogonal to the original axis of launch. Its intensity is given by the following expressions for transmissivity, T_p and phase shift, $\Delta\Phi$:

1. $T_p = \sin^2(\Delta\Phi/2)$
2. $\Delta\Phi = 2\pi L/\lambda(\Delta n_x - \Delta n_y)$

where L is the length and Δn_j refers to the respective nonlinear induced index changes along the axes. Any inherent birefringence is here ignored. Clearly, if the phase change due to the relative delay is π or an odd multiple of π, then the entire incident signal is converted to the orthogonal polarization. A polarizer oriented to block the input signal when no pump signal is present, will then function as an optical gate that passes a signal only when pump light is present. In this, the usual description of the Kerr gate, the high power pump pulse is distinguished from the signal (or probe) pulse. In fact the two need not in general be at the same wavelength. It can be shown theoretically that in this case self modulation still takes place and has a peak transmissivity given by the somewhat more involved expression:

3. $T_p = \sin\{(\gamma/6)P_o L\cos(2\theta)\}\sin^2(2\theta)$
4. $\gamma = \pi n_2/\lambda A_{eff}$

Here θ is again the launch angle, P_o the incident power, with n_2 being the nonlinear index coefficient of the fiber, L its length and A_{eff} the core area. Computations show that although total polarization conversion is not achieved, certain choices of incident polarization orientation angle (θ) and incident power can yield as much as 90 % efficiency. Even for single pass operation, pulse shaping will take place at any value of θ which corresponds to a local maximum of the transmissivity function, because the lower intensity wings will incur relative attenuation. Such effects are enhanced in multi-pass oscillation, resulting in a mechanism which promotes decreasing pulse width in the time domain from each pass of the polarizing gate. Thus an intensity enhanced transmissive state, correlating to a compressed temporal pulse, can become the preferred mode of operation as in the solid state case. Both utilize the Kerr effect somewhat differently, however. The effect can be rigorously analyzed as a polarization evolution, but is sometimes loosely referred to in this context as rotation. We note that although residual inherent or mechanically induced birefringence also generates rotation effects, these are not intensity dependent and are nulled or compensated in operation so as to have no active role in gating effects. It should also be stressed that incomplete switching of the polarization reduces the throughput, but does not preclude switching shutter operation.

$\chi^{(3)}$ COEFFICIENT VALUES

The existence of the nonlinear Kerr effect has of course been established in various media and configurations including fiber: however, it is generally induced at high field intensity. What is unusual in these fiber ring experiments, is the extremely low threshold observed for modelocking effects. It needs to be shown that the required phase shifts or index changes are consistent with known values for the nonlinear coefficients. as well as the optical power levels observed in the fibers in this experiment. This is done below for the case of the distinct pump-signal, but also applies to the case where they are identical.

We refer back to eq. 2 and use the following expressions to give the index changes in terms of the optical field intensity and nonlinear coefficient:

$$\Delta n_x = 2n_2E^2 \text{ Any} = \Delta n_2 bE^2$$

The energy density term (square of the field strength) is related to the propagating optical power and effective fiber core area by: $P = E^2A_{eff}$

Defining the Kerr coefficient as: $n_{2b} = 2n_2$ (l-b)

We take b=1/3 as a good approximation in silica. The value of P required for complete polarization switching (a phase shift $\Phi = \pi$) is given by inserting the above results into eq. 2. The result is: $p = \lambda A_{eff}/2Ln_{2b}$

The value of $n_{2b} = 5xlO^{-16}$ cm/W as has been established in referenced work and $A_{eff} = 25$ μm^2 is typical of the silica fiber core of the erbium doped fiber used in the lasers and amplifiers. Taking $\lambda = 1.5$ μm and L = 40 m, the requirement is: P = 10 watts.

This calculation is for a CW value, whereas in our application the pulsed power value must be used. A sufficiently accurate estimate of this can be based on the assumption that the average laser power (measured on a CW meter) is converted to pulsed power. The peak value is then estimated from the product of the CW value with the ratio of the pulse interval to the pulse width. Taking a few measured combinations from the data:

Period T = 400 ns, Width t = 1 ns, $P_{cw} = 4$ mW
yields: P = 1.6 watts of output power.

T = 400 ns, t = 25 ps, $P_{cw} = 20$ μw yields: P= 3.2 watts
It is clear that the intensities can indeed be in the correct order of magnitude. It is typical in fiber applications that the confinement of the small area core and the long interaction length, compensate (as shown directly in eq. 5) for the relatively low nonlinear coefficients of fiber media. Incomplete switching would result from a lower peak pulse power and there would be an additional loss for each pass. Such losses are compensated if the round trip gain is sufficiently high. A solution of the rate equations would relate this to the overall energy conversion efficiency, which is at this stage not of primary interest.

A unique observation requiring interpretation in terms of such a mechanism is the fact that our results show that modelocked behavior was achieved with or without an explicit polarizing element. This was done by using a polarizing Faraday optical isolator alternatively with a polarization insensitive isolator. No other published work has exhibited such effects without a polarizing element. These considerations do not pertain to the polarization controller (in this case the 3 paddle type) since such a device alters the state, but passes all incident states of polarization without selective loss. Its function here is mainly to set the optimum value of zero. Work is planned to establish whether the pump laser's polarization provides a selection mechanism upon each successive cycle of the lasing signal beam through the ring cavity, or whether some other relatively small polarization response effects are sufficient to induce cavity switching.

CONCLUSIONS

The observations to date are generally consistent with proposed theoretical mechanisms, but more experimental work is required to determine if there are other unidentified contributing effects. Even at this stage, the ring laser here demonstrated entails to our knowledge the simplest self pulsed, passive configuration with the lowest threshold. Other configurations require additional components such as modulators and etalons. This system design is modular and shows significant progress toward the goal of a practical

pulsed or CW fiber laser. A focus for future work is the ability to vary the pulse width and power independently, and to incorporate amplification if needed. This would facilitate a variety of communication and fiber based sensor applications.

An overall assessment based on this work would confirm that polarization sensitivity is a problem for a practical system, particularly when the mechanism of operation also relies on it. Movement, stress and temperature can all affect the polarization and generate long term instability. These problems are overcome in the next fiber laser system using a standing wave cavity which is almost completely insensitive to polarization effects. It is that design which was pursued in further work on pulsed fiber laser sources.

7.2 Self Modelocked Fiber Laser with Saturable Absorber (System #2)

The laser described is an all fiber cavity, producing self starting mode locked pulses (fig.28). It employs a Fabry-Perot (standing wave) cavity with a fiber grating as one reflector and a nonlinear mirror based on a saturable absorber as the other. It operates at a pump power of less than 50 mW and produces mode locked pulses from 6 to16 ps. Remarkably, the entire system except for an electrical power supply can be packaged in a metal box of 1x3x5" dimensions.

BACKGROUND

Modelocked fiber lasers have generally utilized ring and "figure 8" configurations rather than Fabry-Perot cavities because the latter required the use of external reflectors difficult to incorporate in optical fiber systems. The development of fiber grating technology has changed this, since the exposure of phase gratings into the core of single mode fibers is now a well established technicalnology[4]. Using this process, it is possible to produce gratings with a wide range of reflectivities and band passes of several nanometers at wavelengths of high fiber transparency. To date most of this work has concentrated on the development of ultra narrow line output lasers. However, the band pass of these Bragg gratings can be made large enough to allow spectral line widths compatible with pico-second range mode locked operation. In fact the actual fabrication requires less time and expense. Modelocking in such a laser is then achieved by the use of a non linear mirror constructed from multiple quantum wells on an indium phosphide substrate. Quantum well saturable absorbers have been used to mode lock bulk solid state lasers[6,7] and recently used to mode lock both erbium doped[8] and neodymium doped[9] fiber lasers. The self starting threshold achieved in this work was low compared with other reported fiber laser systems. The pump power of 30 to 45 mw can be obtained from a moderate power 980 nm diode laser.

EXPERIMENTAL RESULTS

The layout of the standing wave laser is shown in Fig 1. To simplify the construction a commercial gain module was used as the gain medium. This module contained about 20 meters of erbium doped fiber pumped at 980 nm by a pig tailed semiconductor laser. It

had a maximum small signal gain at 1.53 nm of about 30 dB, at a pump laser current of 200 mA, which corresponds to approximately 45 mW of launched pump power. Several fiber gratings (fig.30) exposed onto standard single mode telecommunications fiber, were fusion spliced onto the input fiber of the gain module and served as an end reflector in the standing wave cavity. The peak reflectivity of the fiber grating was 90% centered at 1.524 nm with a pass band width of 0.20 nm. Outside of this region the grating was transparent. The output fiber from the gain module was angle cleaved to prevent back reflections and initially mounted at the focal point of a 10 power microscope objective. Collimated light from this objective was focused with a second microscope objective onto a quantum well saturable mirror, which served as the other end mirror in the standing wave cavity. This configuration was eventually replaced by simply bringing the cleaved fiber into near contact with the MQW surface (fig.38). One integrated version incorporated a MQW chip (≈2x2mm) permanently laminated to the fiber tip.

MQW SATURABLE ABSORBER

The quantum well mirror consisted of 50 alternating layers of AlInAs and GaAlAs deposited on an InP substrate (fig.27). The total thickness of these layers was 1.0 μm , while the substrate was 1 mm thick. The device was mounted so that the surface containing the quantum well structure was on the inside of the laser cavity. The linear transmission of this mirror was 0.18 at 1.524 mm (fig.31). Mode locking was sensitive to the lateral position of the quantum well mirror. Changes in position of the order of 10 mm could initiate or eliminate mode locked pulses. Measurements (fig.28,29) of the optical spectrum of the laser were made with a scanning spectrum analyzer with a resolution of 0.1 nm. The temporal behavior of the laser was observed both with a fast InGaAs photodetector and a special (Inrad) diode model autocorrelator. Most of these measurements were made through the fiber grating, as shown in the diagram. The loss resulting from transmission through the MQW was eliminated by depositing a highly reflective gold coating on the rear surface. Ultimately, the MQW growth process could include a dielectric reflective stack composed of similar materials. An average power of 2 mW was measured at the output .

DATA

The output pulse train was stable and self-starting at a low threshold of 30 mW; at 50 mW pump power, the pulse energy was between 1 and 2 nj at 1.55 μm.

System with Bragg Grating:	**Fiber Grating #1**	**Fiber Grating #2**
Grating Tx Bandpass	**0.3 nm**	**1.5 nm**
Pulse Spectral Width	**0.15 nm**	**0.3 nm**
Pulse Temporal Width	**16.5 ps**	**8.0 ps**
Time Bandwidth Product	**.314**	**.305**

DATA ANALYSIS

It is clear that the choice of fiber grating spectral width directly influences the resulting spectral width of the pulse. We further note that each grating yielded a similar transform limited time bandwidth product {.315 for $sech^{-1/2}$ pulse shapes}. This in turn implies an inversely proportional temporal pulse width, which is precisely what was observed. The results are quite satisfying and would indicate that the pulse width can be tuned (or selected) by the selection or tuning of the fiber grating. The extreme limits of this process would justify testing in future work. This laser has also demonstrated progress toward a portable and alignment free pulsed fiber laser source for signal processing applications and field use.

When the saturable mirror was properly aligned, the laser produced a stable train of mode locked pulses as shown in Fig 2. The period of these pulses was 308 ns with a frequency of 3.25 MHz. An auto correlation trace of these output pulses is shown in figure36. If it is assumed that the pulse shape is hyperbolic secant, the pulse width obtained from this data is 16.5 ps. The resultant output spectrum, measured at maximum module gain is shown in figure 28. This spectrum was very stable during the sampling time of the spectrum analyzer. It consisted of two bands whose relative heights depended strongly on the alignment of the components of the cavity. The width of each line was 0.17 nm, with a peak to peak separation of about 0.2 nm.. It should be noted that the peak of this spectrum lies at the center of the reflectivity band of the fiber grating Since the resolution of the spectrum analyzer was nominally 0.1 nm, the true spectral line width was 0.15 nm.

DISCUSSION

The long period, or low frequency, of the mode locked pulses shown in Fig. 4 is due to the long cavity length employed in the laser. The gain module used in this work was based on erbium doped fiber of about 20 m. in length. Another 5 m of fiber was used to construct the external portions of the Fabry Perot cavity. Conventional theory states that the frequency of a train of mode locked pulses is equal to the temporal mode spacing of the laser cavity. In a Fabry-Perot cavity of length d, containing a material with index of refraction n, this spacing is given by:

$nf = co/2nd$

Taking $d \sim 25$ m and $n \sim 1.60$ this gives for the mode separation:

$nf \sim 3.75$ MHz

This result is in agreement with the pulse frequency indicated in Fig. 4.

The full width at half maximum of the correlation trace shown in Fig. 5 is seen to be 25 ps. If a hyperbolic sech shape is assumed, this corresponds to an actual pulse width of 16.25 ps. The spectral line width indicated by Fig. 3 is 0.15 nm or 1.93 x 1010 Hz. Thus the time bandwidth product of the mode locked pulses was 0.314 in good agreement with the transform limited product of 0.315 associated with the hyperbolic sech shape.

The auto correlation trace also shows the presence of a broad background of second harmonic signal, indicating that the output of the laser contained some DC component.

The low frequency of the mode locked pulses results in a relatively high peak power for a given average output power. If all the output power of the laser is in the pulses of width t and frequency nf, their peak power relative to the average output power is given by:

$P = (nf/t)Pave \sim 40$ W.

Finally, it should be noted that the quantum well structure employed as one mirror in this laser can either be operating in transmission as a saturable absorber or as a mirror whose reflectivity is modulated by non linear index changes produced by the high intensity mode locked pulses.

The all fiber construction of this laser lends itself to field applications such as the incorporation as the source in a single mode fiber Optical Time Domain Reflectometer. The distance resolution in the sub millimeter range improves on conventional diode laser sources by two orders of magnitude. Tests on signal averaging times required due to the lower pulse energy would require further testing.

CONCLUSION

The transform limited experimental results for the Time-Bandwidth Product highlight one of the primary advantages of fiber laser sources over the presently established laser diode technology. First of all, pulses shorter than tens of pico-seconds cannot be readily obtained from direct drive diode lasers. Furthermore, the intensity dependent gain causes significant frequency chirp, and precludes transform limited performance as was analyzed in section 5. Residual dispersion in actual fiber systems then entails additional pulse broadening upon propagation. Future systems at extremely high data rates may therefore require the advantageous performance of modelocked fiber laser sources. This applies particularly if they can be as rugged and compact as those developed in the course of this project work. Further key issues such as increased repetition rate and synchronization will be investigated in the following section. The results even at this point have demonstrated very significant progress toward practical pulsed fiber laser sources.

7.3 Synchronization of Modelocked Fiber Lasers

The preceding content in this section has described two passively modelocked systems developed at Rome Laboratory. An actively modelocked fiber laser design has also been established here. The assembly was originally initiated in conjunction with Dr. Richard Fork at RPI. A description of that design is not central to this project, however a diagram of the system is given in figure 34. Because there are certain performance tradeoffs in the two laser types, it was decided to attempt a synchronization experiment that could combine the performance advantages of both.

One drawback of a passive approach is the generally lower repetition rate dictated by the relatively long cavity length of most fiber lasers. In an actively modelocked system, it is straightforward to modulate the induced rep rate at any higher harmonic of the fundamental rate, for which driving electronics are available. Thus the active laser can generate rates in the tens of GHz range. The best short pulse performance is, however, most simply achieved in a passive system, with an appropriate nonlinear mechanism incorporated as was done in the two systems described. A combination of these two characteristics would be highly desirable.

Injection Seeding

For many distributed signal applications it would be highly advantageous to have sources that can share a common time base. This can be done optically if one laser can injection seed several others, thereby effectively synchronizing the output pulses of all the lasers and providing a common "clock". There will of course be a constant delay between any two sources, but this can be easily determined and factored out.

This experiment was done by injecting pulses from the active fiber laser into the passively modelocked one, and observing when the separate output from both lasers displayed pulses simultaneously on a singly triggered oscilloscope (fig.35). This experiment was successful and the traces are shown in figure 37. To our knowledge this is the first time this was done with two such fiber lasers. We became aware that another group had done this with a semiconductor laser and a fiber laser with similar motivations. The other significant point was that the passive laser still produced short pulses but at the high harmonic GigaHertz rate of the active laser. The advantageous properties of both were thus combined!

Temporal Stability Analysis

Temporal noise had been analyzed in an active/passive diode based laser in section 4. It had there been observed that the passive laser version displayed greater temporal instability. It was critical to see if this was also the case here. Similar noise measurement calculations were made on a frequency spectrum analyzer. The results (fig.39) showed a surprisingly low value for the passive timing jitter (fig.33). It also showed the effect of the natural relaxation oscillation at approximately 7 kHz. This is very good news for the applications perspective, since the sub-picosecond timing stability (fig.32)indicates a limit approaching a tera-Hertz in the signal rate. The Conclusion to be drawn from these results is that the fiber based gain medium does not incur intensity dependent gain, in contrast with the semiconductor gain media analyzed in section 4. For this reason the temporal and amplitude stability are both excellent even in a passively modelocked fiber laser source.

Conclusions

Fiber based sources pulsed have been developed to the point where they are almost sufficiently portable and compact for field use. Previous developments at other locations have achieved this in CW versions for applications such as fiber gyroscopes an CATV. What is new is the ability to produce modelocked pulses for digital signal applications in systems that are reasonably rugged and free of alignment and polarization problems.

Fiber laser sources have recently been developed to the point where their theoretical performance advantages over diode based laser sources can be realized in practice. Much further work is needed, however, in modulation methods and in reducing costs of components, particularly pump lasers. This will be essential for widespread use in applications outside of the laboratory.

8.0 REFERENCES

1. E. P. Ippen, H. A. Haus, and L. Y. Liu, J. Opt. Soc. Am. B6, 1736 (1989)
2. N. J. Doran and D. Wood, Opt. Lett. 13, 56 (1988)
3. K. J. Teegarden, R. K. Erdmann, S. Qazi, SPIE Symposium OE/Fibers, Boston, 1992
4. T. Erdogan and V. Mizrahi, "Fiber phase gratings reflect advances in light wave technology," Laser Focus World, pp. 73-80, February 1994.
5. V. Mizrahi et al., "Stable single mode erbium fiber - grating laser for digital communication," J. Light wave Technical., Vol. 11, No. 12, 1993.
6. Keller et al, "Coupled-cavity resonant passive mode-locked Nd:yttrium lithium fluoride laser", Opt. Lett., Vol. 19, pp. 390-392, 1991.
7. Keller, et al, "Solid-state low-loss inter cavity low loss saturable absorber for Nd: YLF lasers: an anti resonant semiconductor Fabry-Perot saturable absorber", Opt. Lett., Vol.17, pp. 505-507, 1992.
8. W. H . Loh, et al, "Passively mode locked Er3+ fiber laser using a semiconductor nonlinear mirror," IEEE Photon. Technical. Lett., Vol. 5, No. 1, pp. 35-37, January 1993.
9. W. H. Loh et al, "Diode-pumped self starting passively mode locked neodymium-doped fiber laser," IEEE Photon. Technical. Lett., Vol. 29, No. 9, pp. 808-809, April,1993.

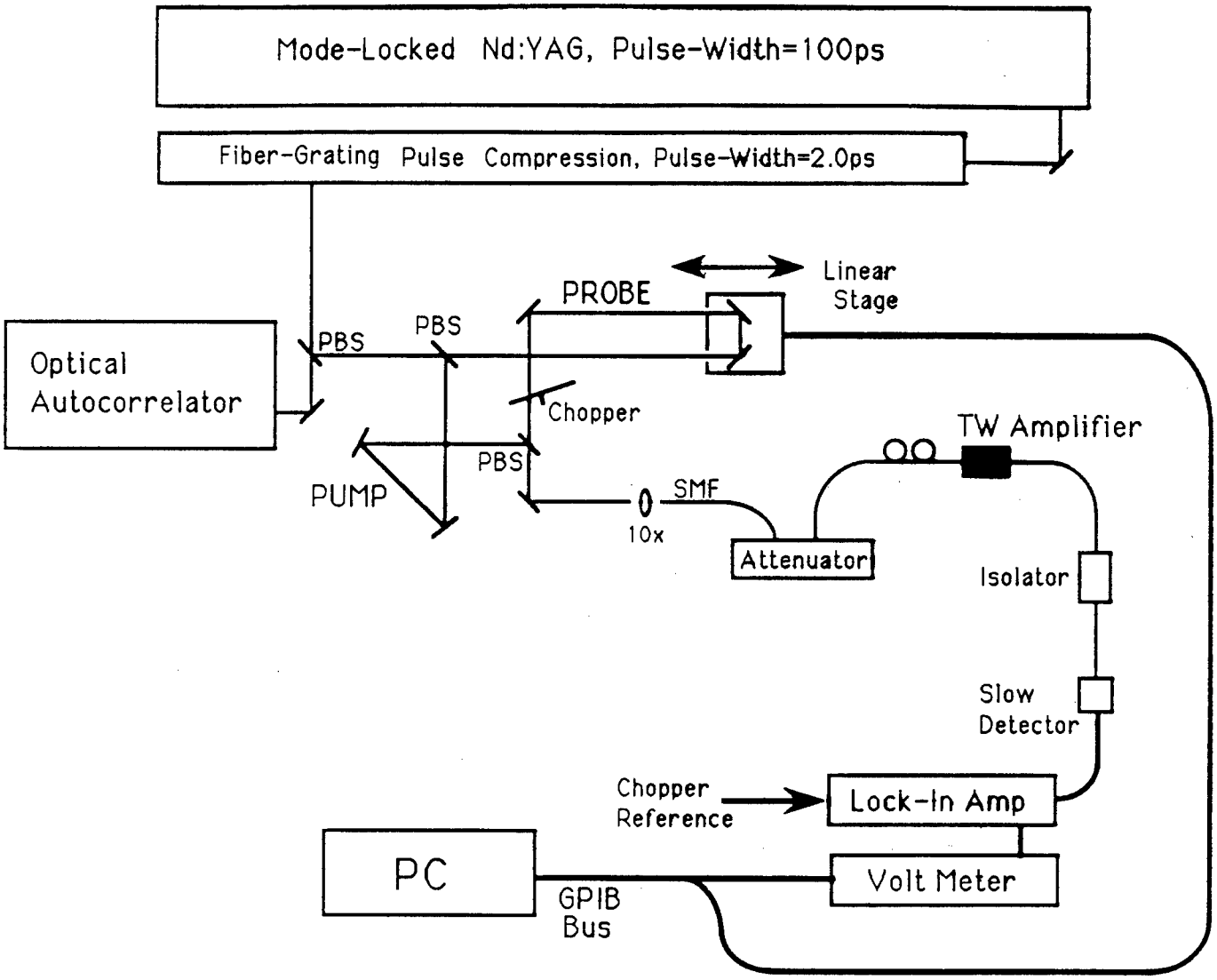

Pump/Probe Amplifier Test System
Figure 1

STAR COUPLED ARCHITECTURE

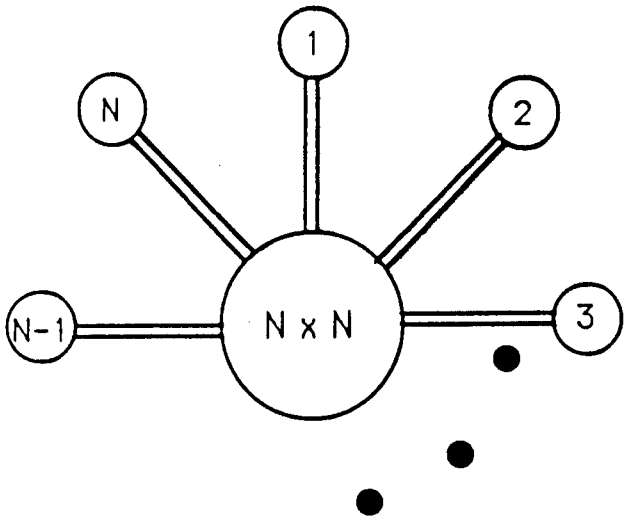

TWLA Application in High-speed Demultiplexing

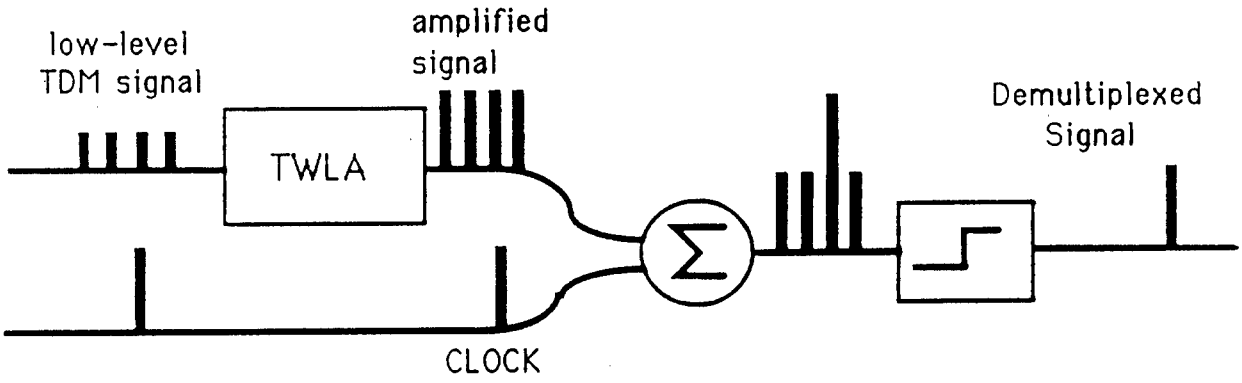

Other Applications to TDMA Architectures

1) Loss compensated coupling and splitting

2) Demultiplexing
   a) Enhanced optical threshold detection
   b) Increased excitation energy for nonlinear device detection

Figure 2 TDMA System Architecture

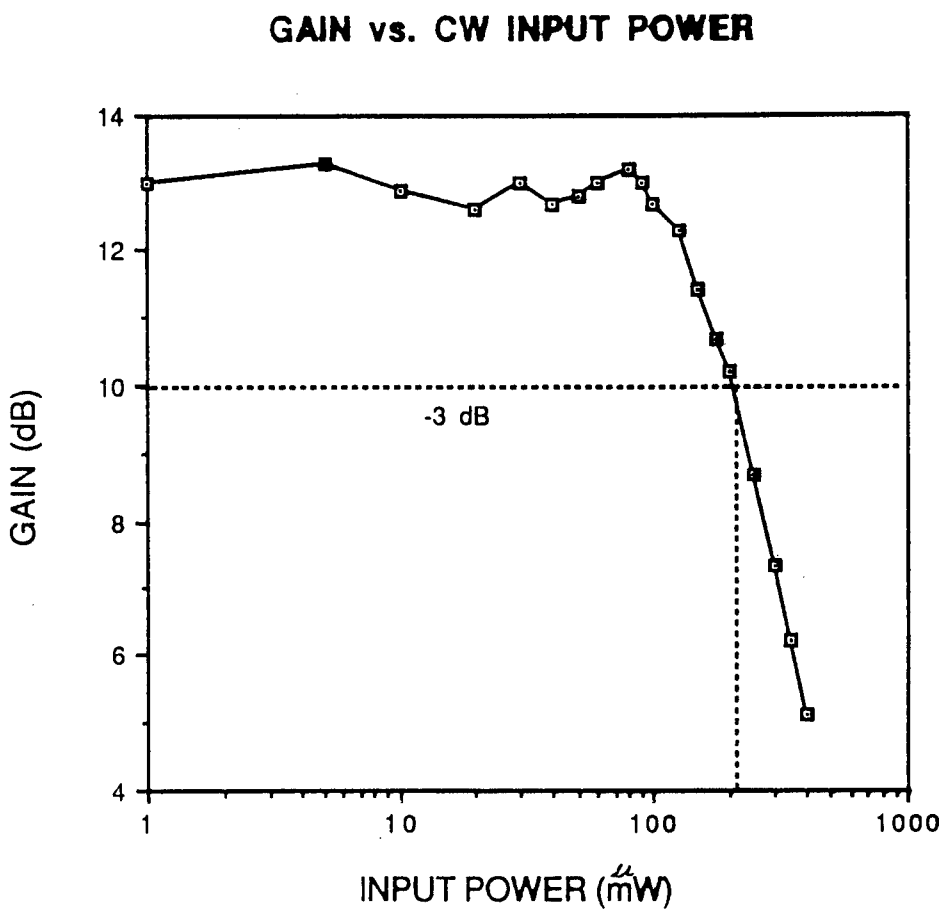

Figure 3. CW Gain vs. Input Power

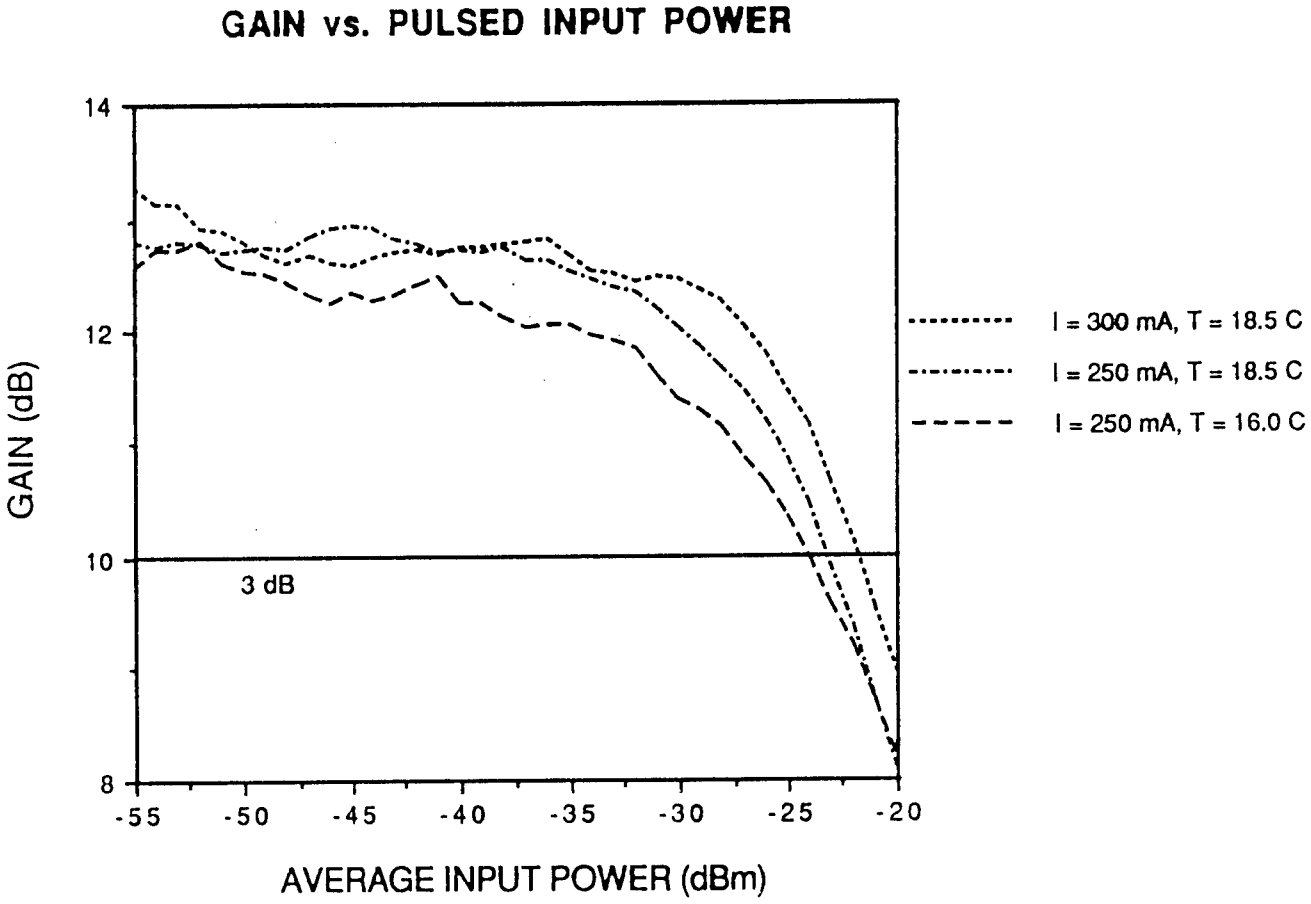

Figure 4. Gain vs. Pulsed Input Power

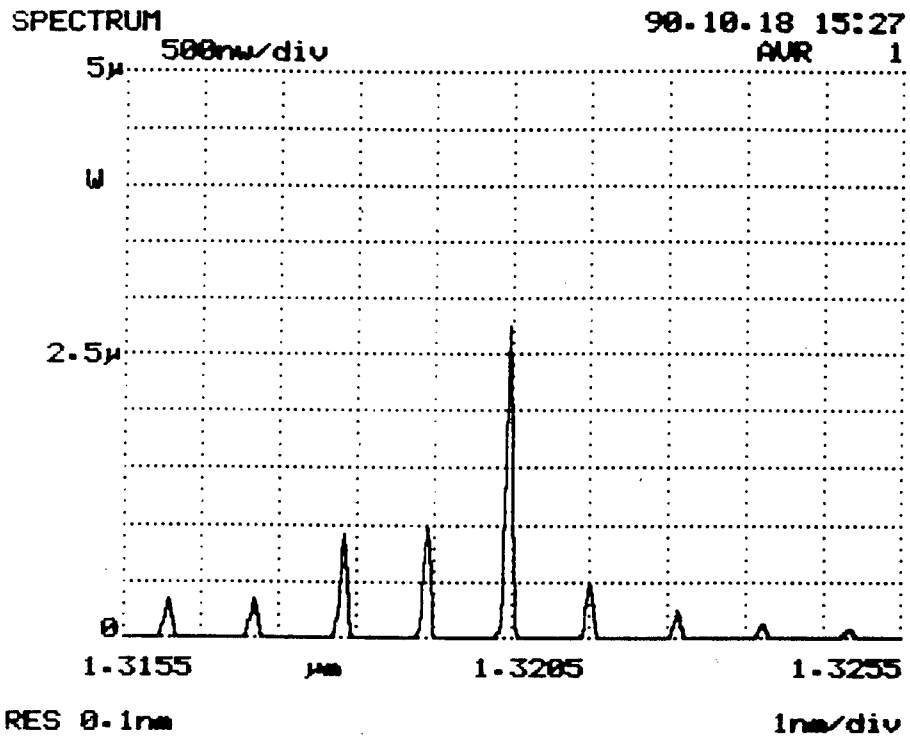

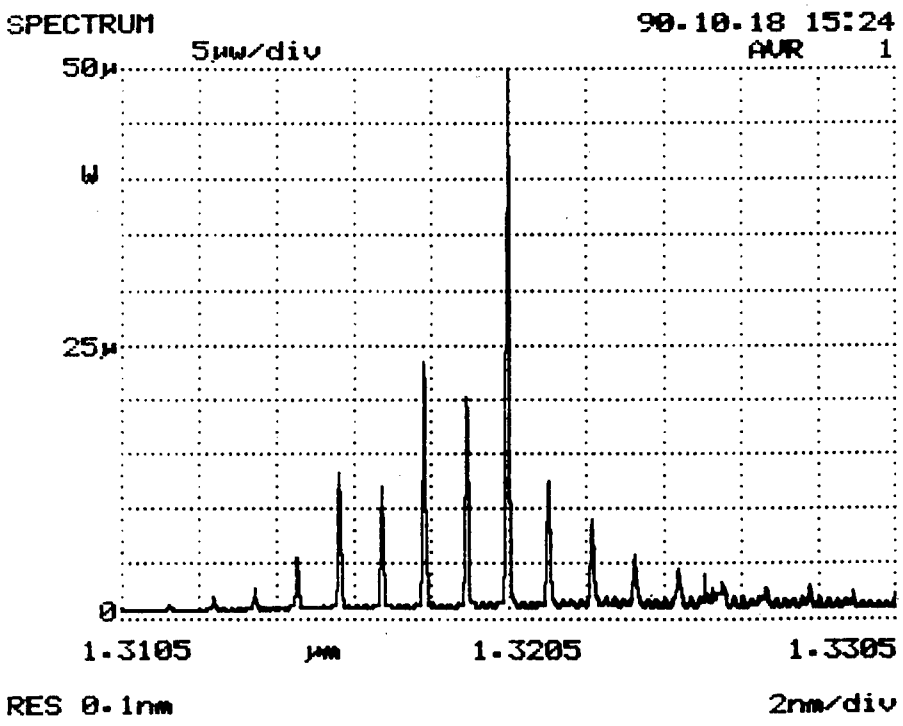

Figure 5. CW Spectrum Before and After 13 dB Amplification

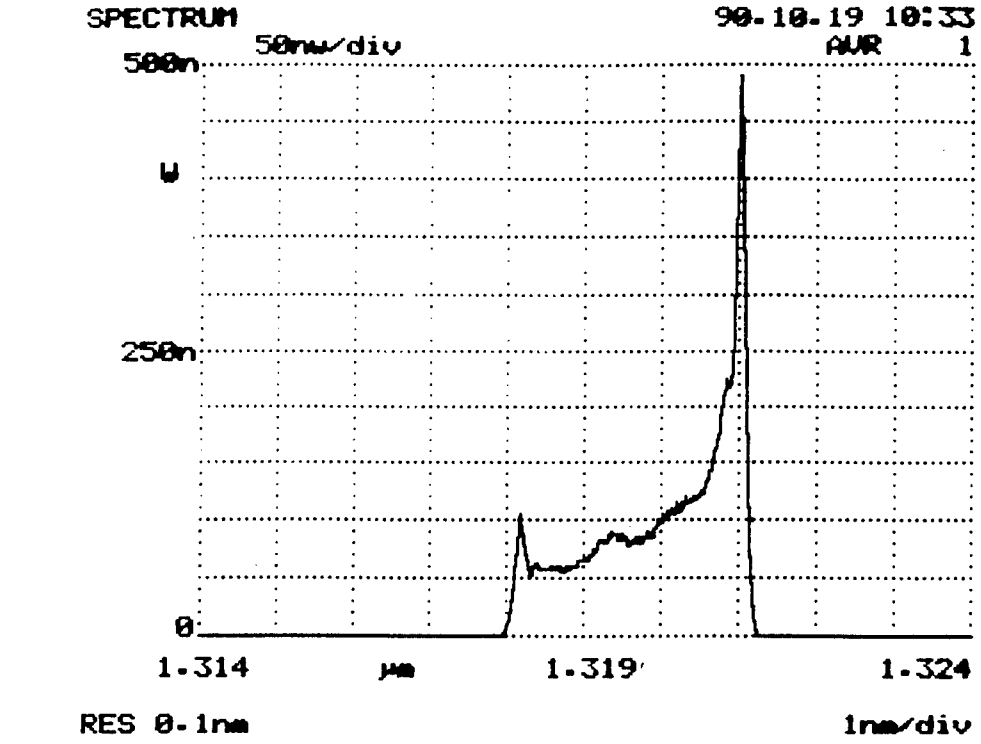

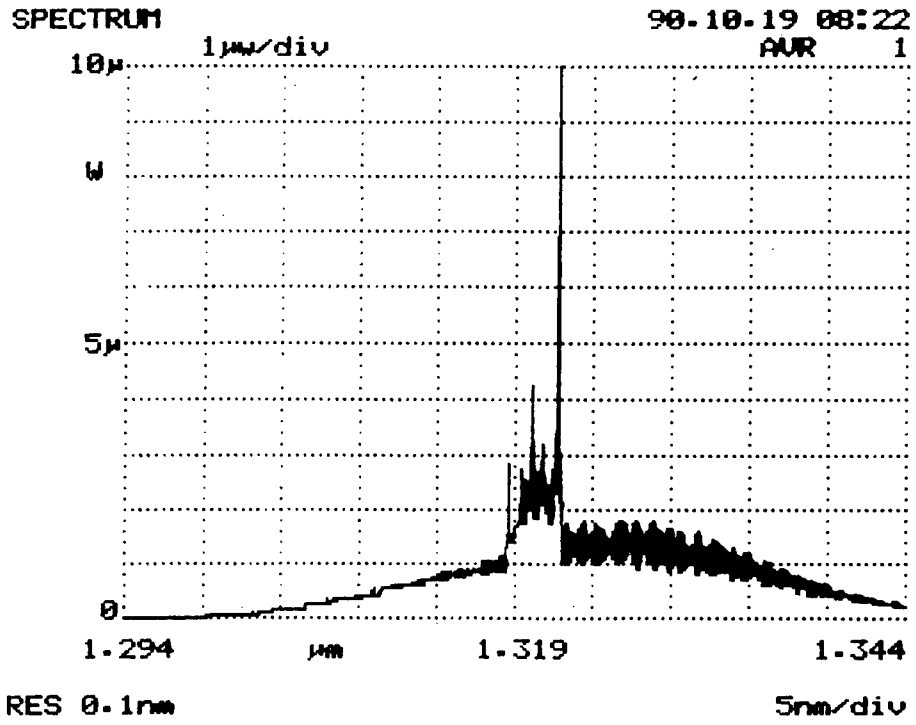

Figure 6. Pulsed Spectrum before and After 13 dB Amplification

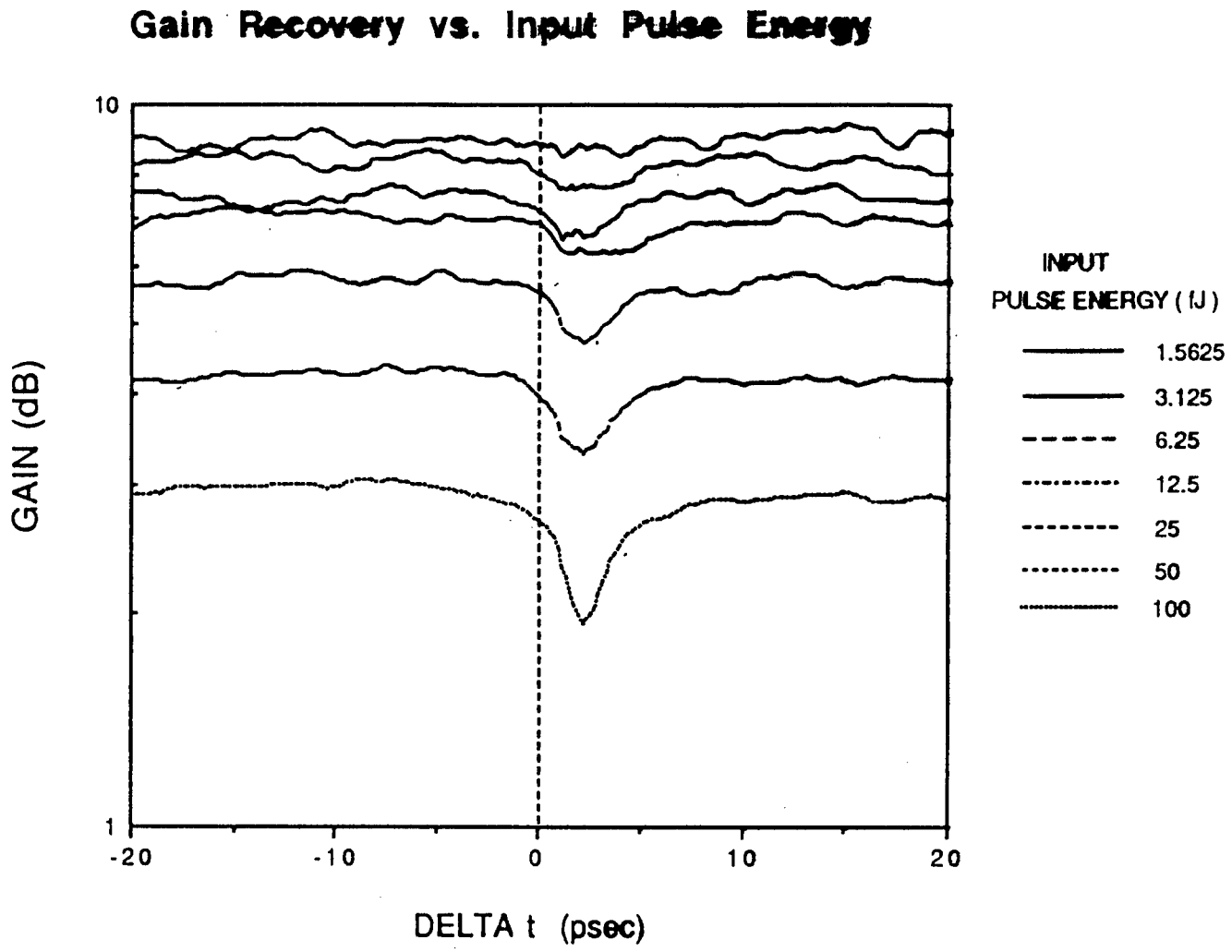

Figure 7. Gain Recovery vs. Pulse Energy

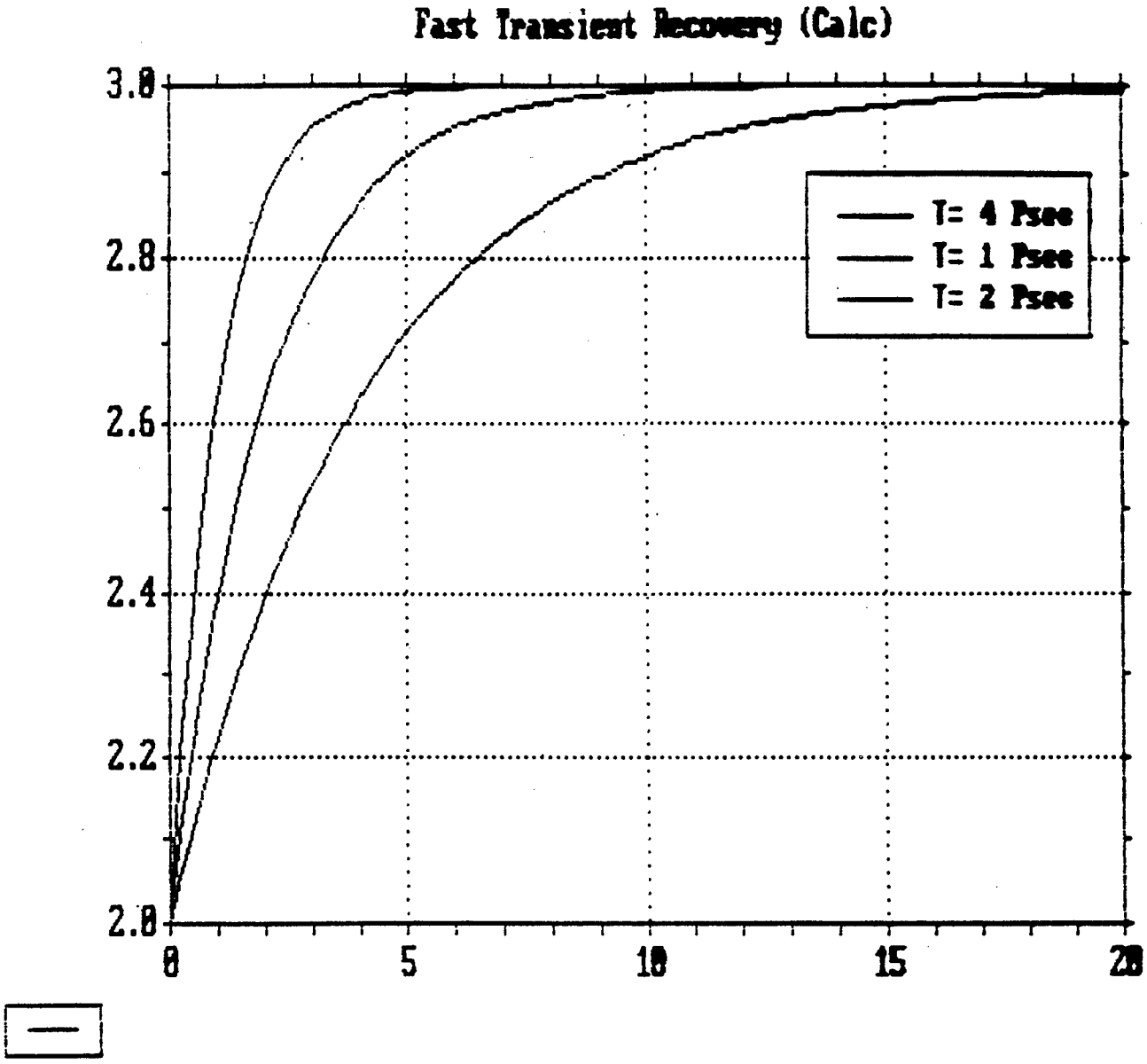

Figure 8. Transient Gain Recovery --Calculated

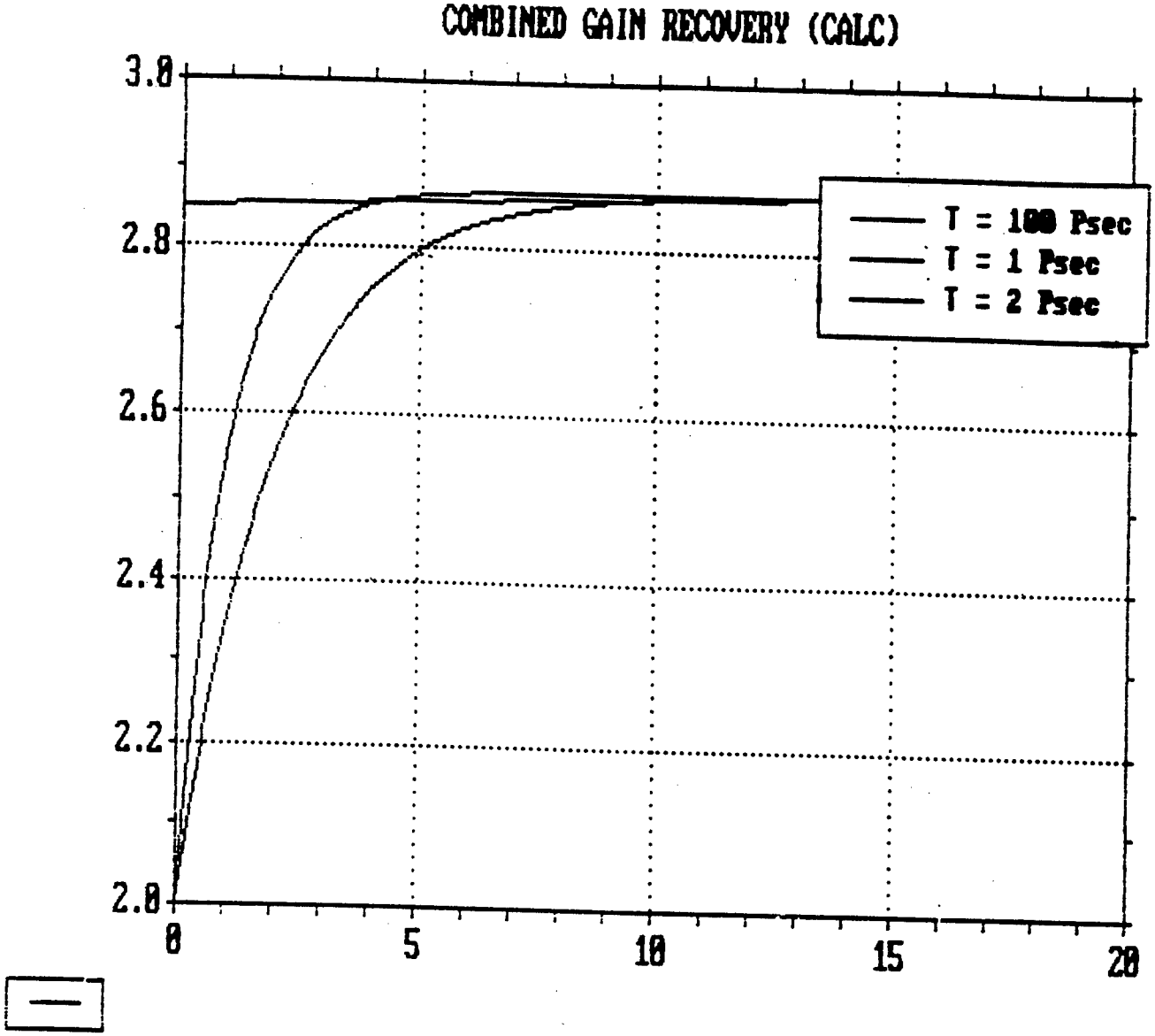

Figure 9. Combined (Fast and Slow Time Constant)--Calculated

2 - LEVEL MODEL (SIMPLIFIED)

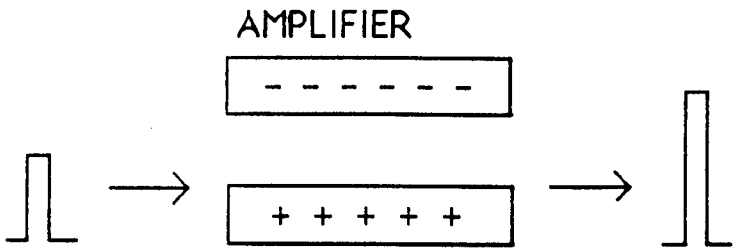

$E_{in} = n(h\nu)$ $\quad N_2 - N_1$ = inverted carrier population $\quad E_{out} = gn(h\nu)$

$h\nu$ = photon energy

g = gain(small signal)

CASE 1) $\quad T(\text{recovery}) \gg t(\text{period})$

Max Pulse Energy Out $\quad E_{max} = (N_2 - N_1)gn(h\nu)$

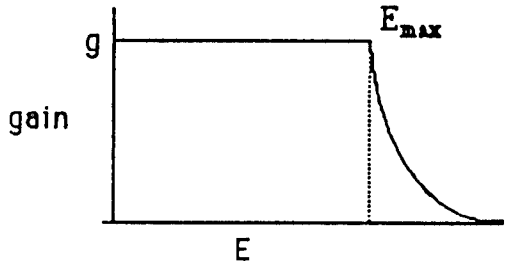

CASE 2) $\quad T = t$ (optimized)

$E_{out} = E_{max}$

All input energy experiences full gain and amplifier is used continuously at full capicity.

$$P_{ave(max)} = \frac{E_{max}}{T}$$

$$P_{3\,dB(CW)} = \frac{E_{3\,dB(pulsed)}}{T}$$

Figure 10. Two - Level Model for Pulsed Gain Saturation

$$E_{sat} = \frac{h\nu}{2S}\frac{A}{c} = \frac{h\nu ALN}{.23g}$$

UNITS OF JOULES, SEC, MICRONS

A = area	1
S = gain crossection	
l = length	1000
g = small signal gain	300
N = carrier density	10^6
h = Plank's constant	6.6×10^{-34}
ν = frequency	2.3×10^{14}

$$E_{sat} = 3 \text{ pJ}$$

SUMMARY OF MEASURED VALUES
(Output Facet of Amplifier)

$$E_{3\text{ dB compression}} = 1.0 \text{ pJ}$$

$$P_{\substack{ave \\ 3\text{ dB compression}}} = 6.5 \text{ mW}$$

$$P_{(\text{peak pulsed})} = 500 \text{ mW}$$

$$P_{(\text{peak density})} = 50 \text{ MW/cm}^2$$

$$T \cong \frac{E_{3\text{ dB}}}{P_{\substack{ave \\ 3\text{ dB}}}} = 150 \text{ psec}$$

Figure 11. Performance Data Summary--Semiconductor Amplifier

CONCLUSIONS

1) Fiber to fiber gain of over 13 dB for the 1.319 micron CW case and 2.0-psec pulsed case.

2) Useful bandwidth range is described through the application of a simple 2-level model.

3) Recovery time inferred from 2-level model consistent with pump-probe measurements.

4) At signal periods of a few picoseconds or at high peak powers nonlinear device behavior becomes predominate.

5) A TWLA can be used in ultra-high (> 10 Gb/s) data rate TDM interconnect applications.

Figure 12. Conclusions for TWLA

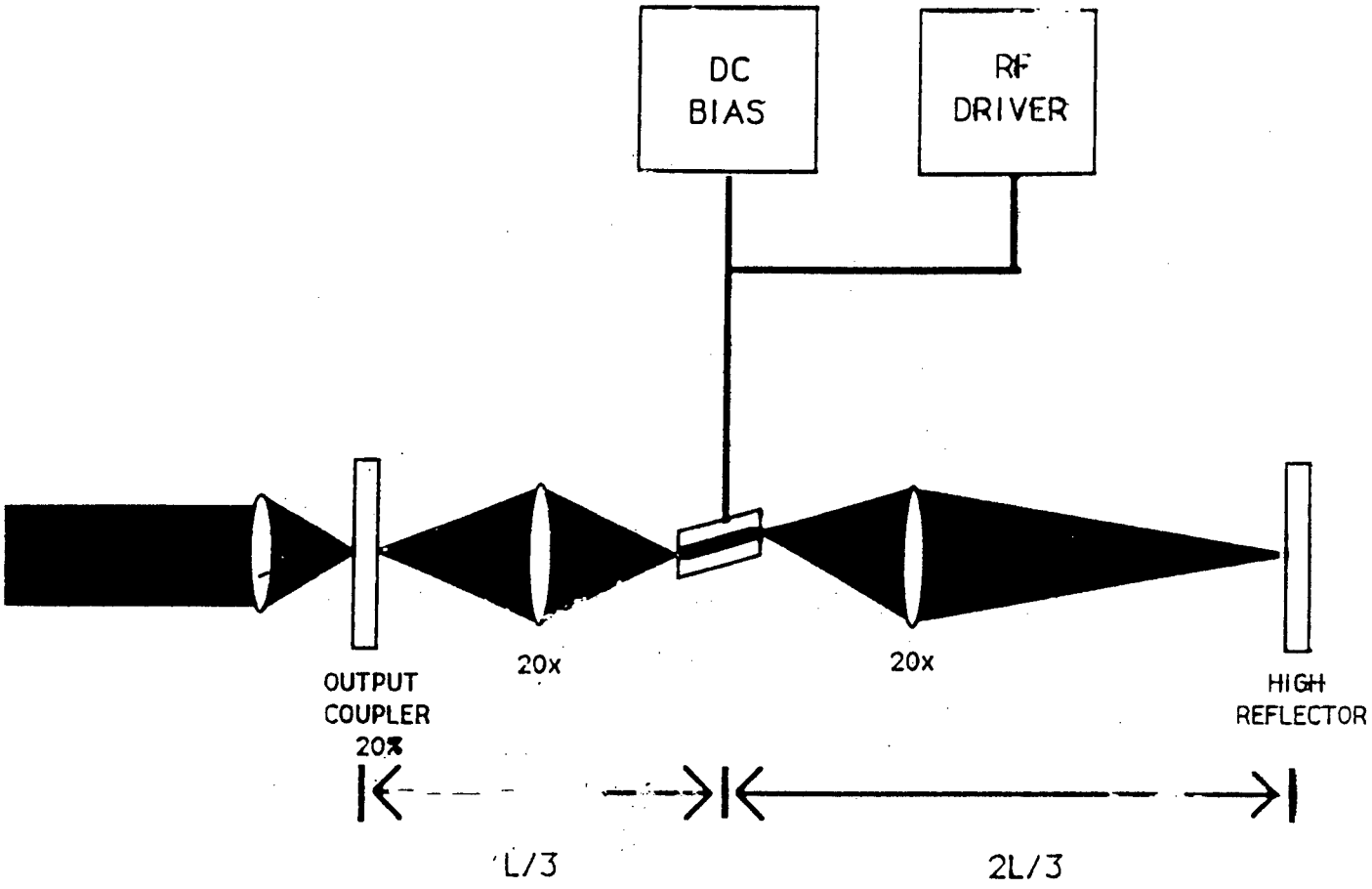

EXTERNAL CAVITY SEMICONDUCTOR LASER

Figure 13. External Cavity Semiconductor Laser Source

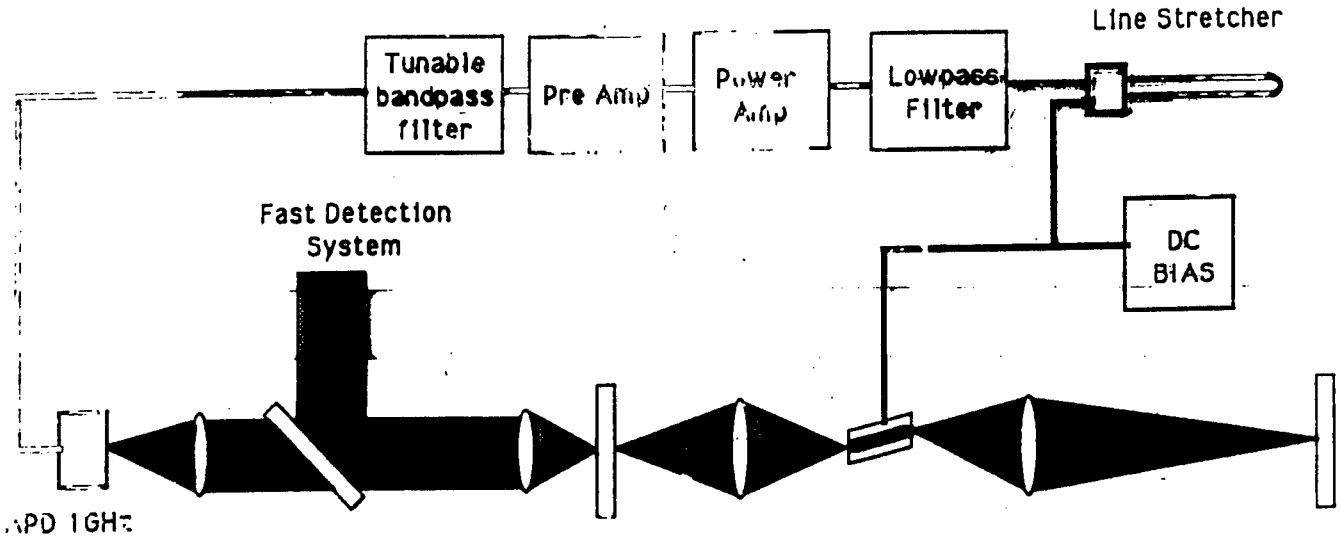

REGENERATIVE FEEDBACK LASER

Figure 14. Regenerative Feedback Laser

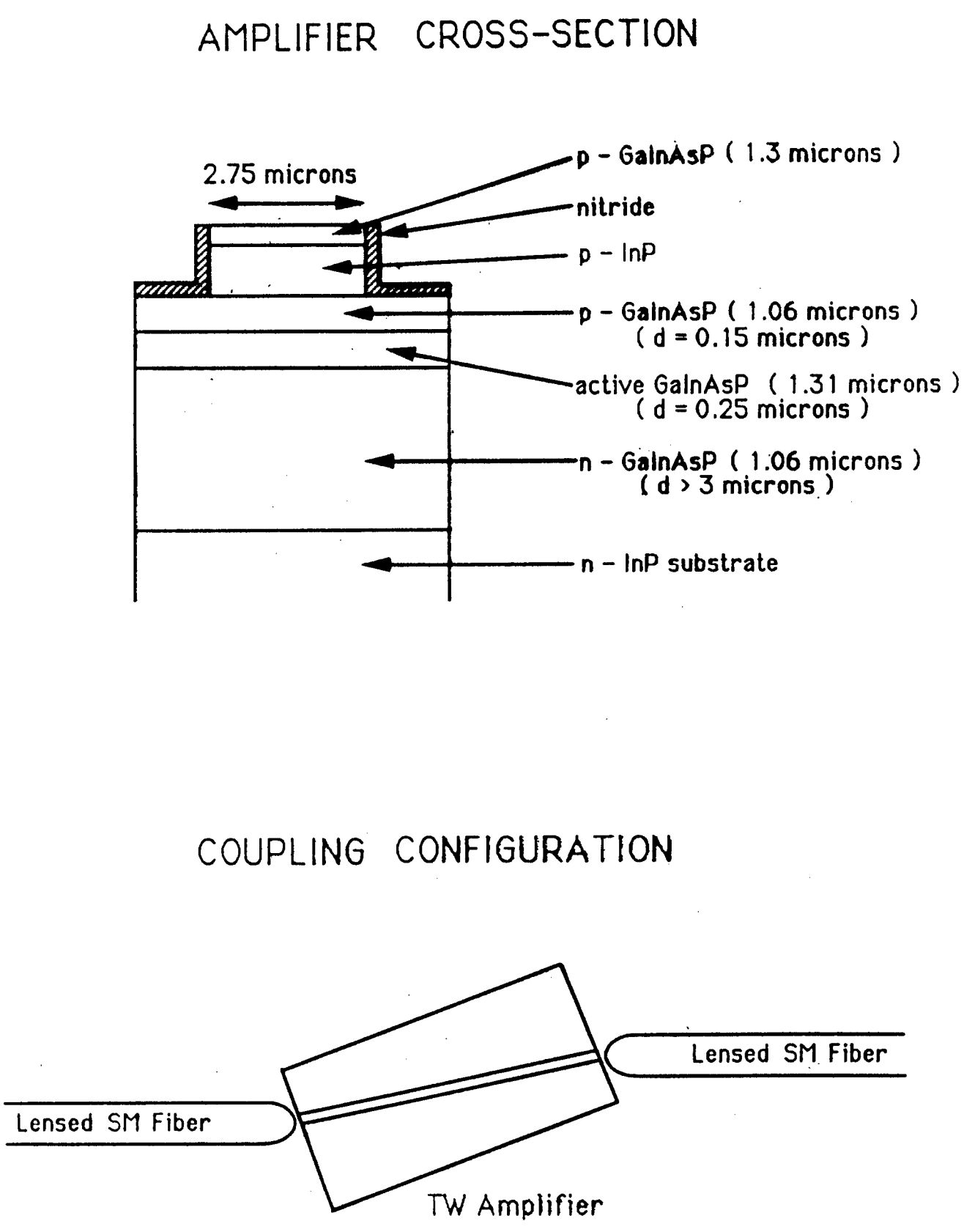

Figure 15. Amplifier Chip Cross-Section and Coupling Configuration

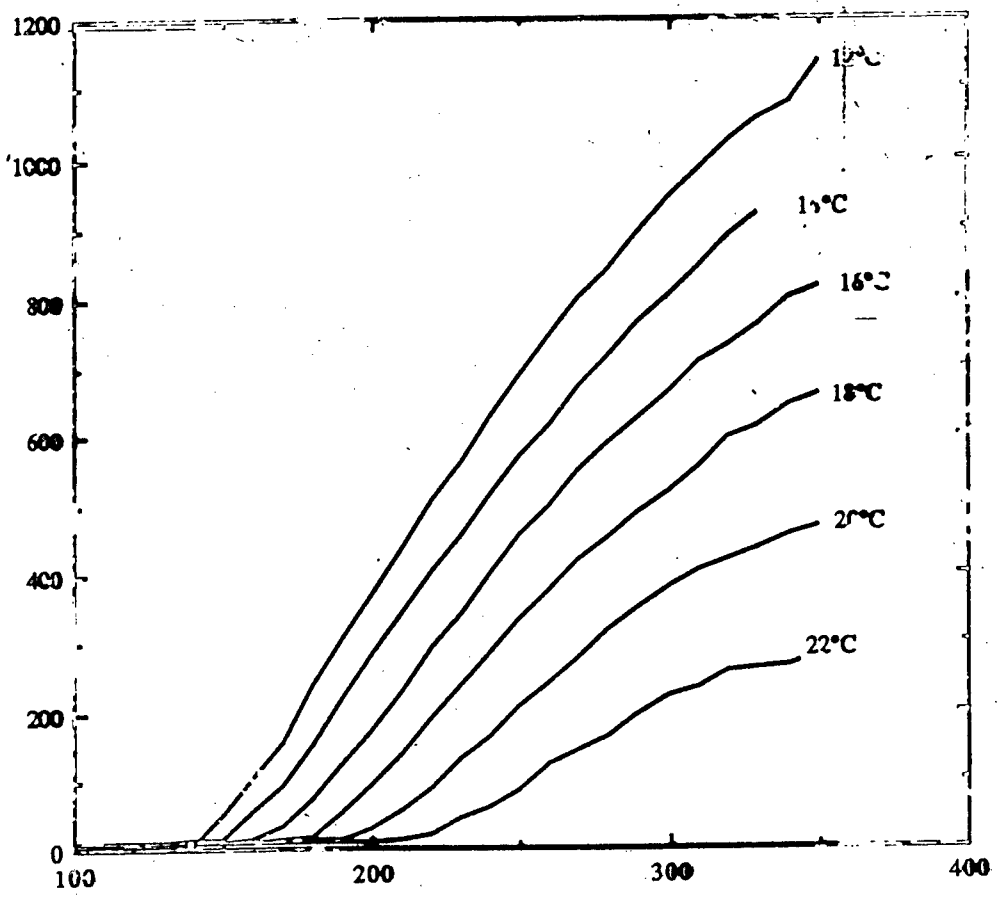

Figure 16. Diode Laser Output Power vs. Drive Current

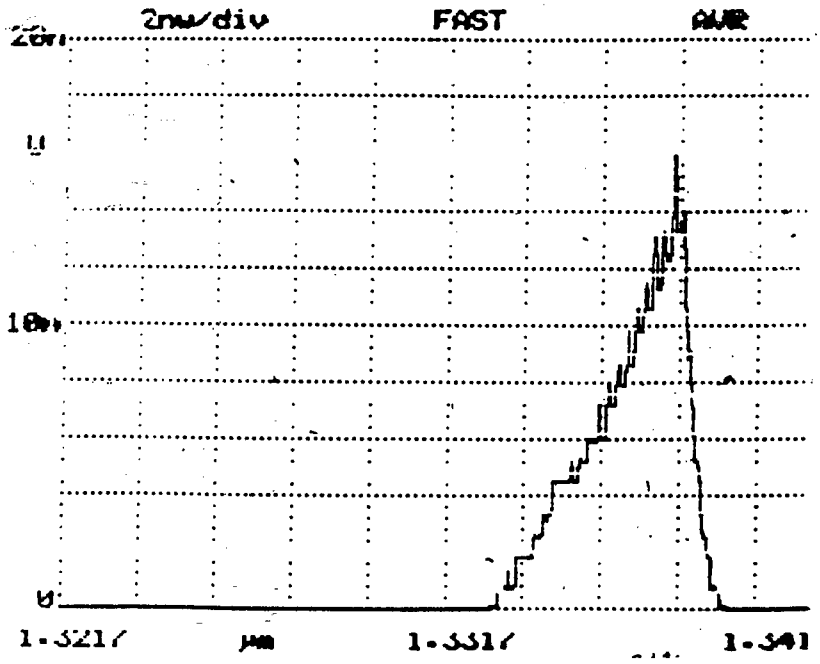

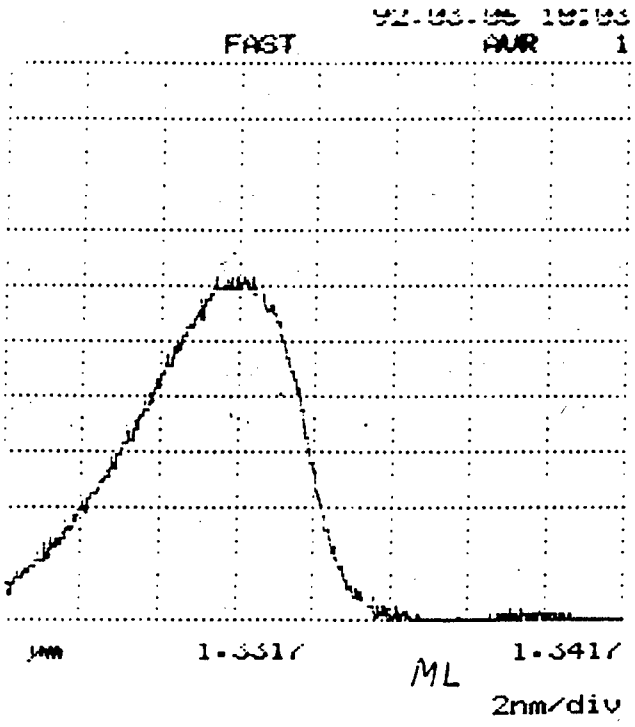

Figure 17. Spectral Output CW (continuous) and ML (modelocked)

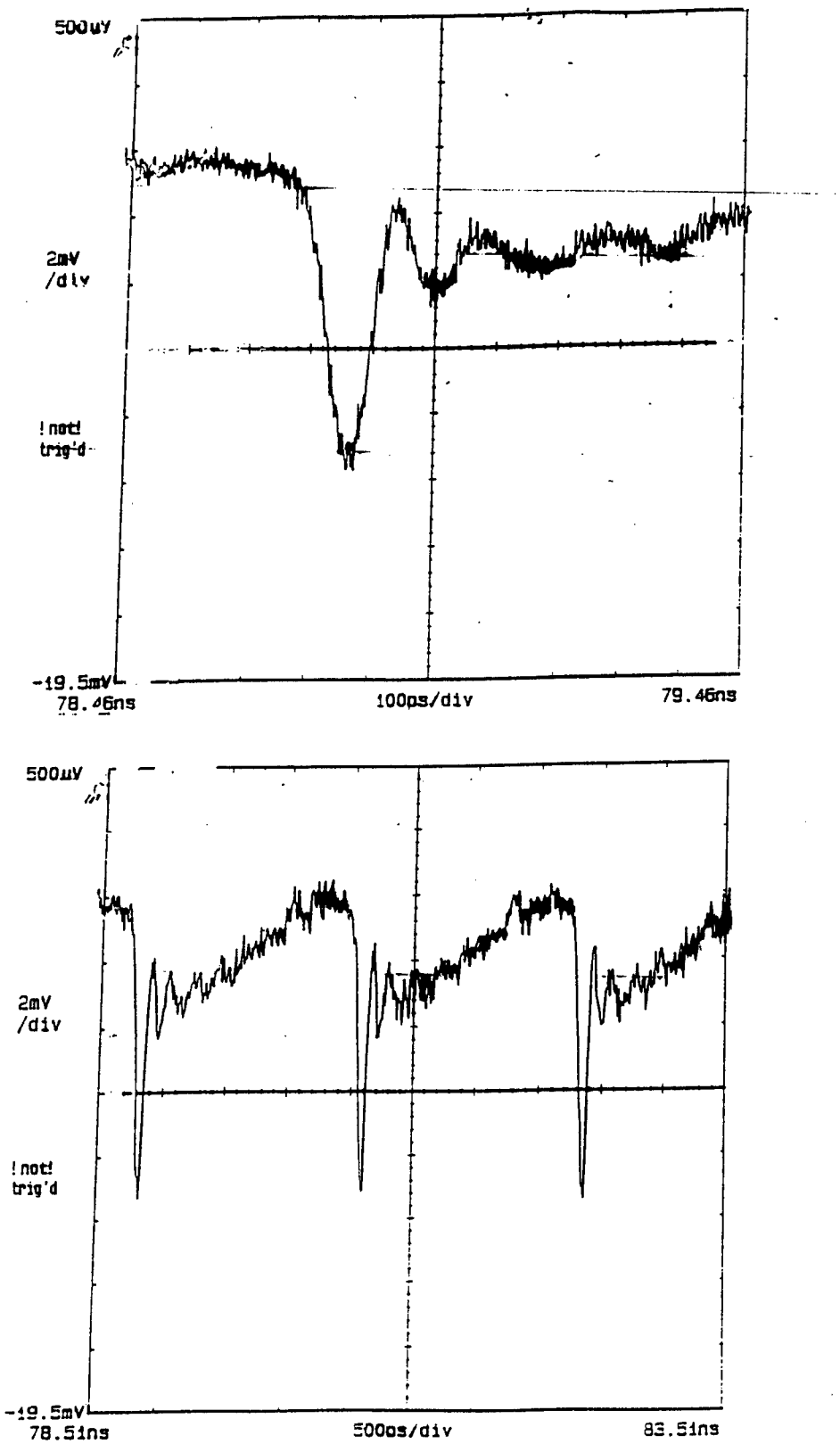

Figure 18. Oscilloscope Trace of Actively Modelocked Pulse Train

PULSE WIDTH CALCULATION

Assuming :

(ACTIVE HARMONIC AMPLITUDE MODULATION)

$$\tau = 0.45 \left(\frac{g}{\Delta m}\right)^{1/4} \left(\frac{1}{f_m \Delta f}\right)^{1/2}$$

For this application:

g	=	round trip saturated gain	1.0
Δm	=	modulation depth	1.0 (ideal)
f_m	=	modelocked frequency	600 MHz
Δf	=	$\frac{c(\Delta\lambda)}{\lambda^2}$	7.1×10^{11} Hz (using $\Delta\lambda$ = 4 nm)

YIELDS :

PULSEWIDTH τ = 22 psec

Figure 19. Theoretical Pulse Width Calculation

Frequency Noise Spectrum

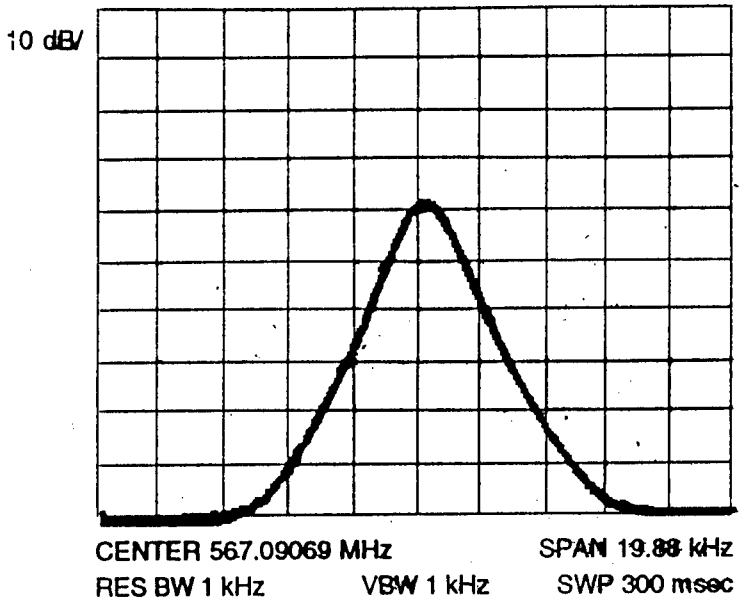

Active Mode Locking

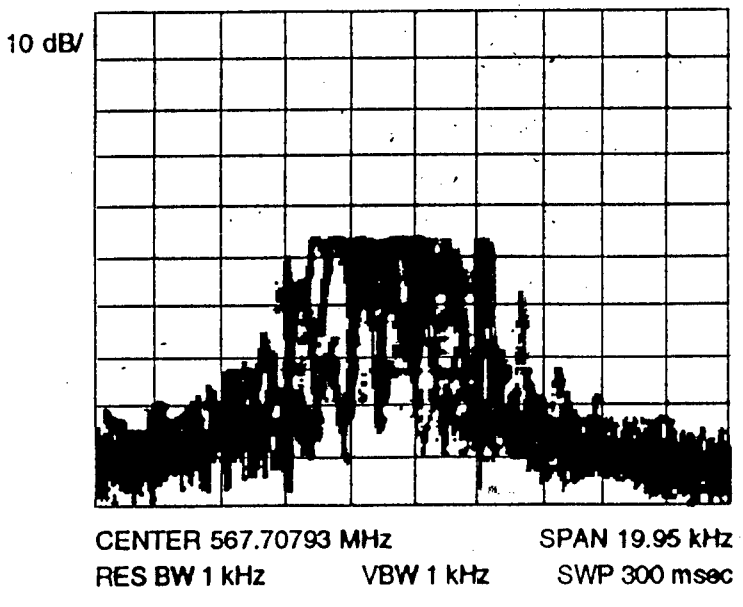

Regenerative Mode Locking

Figure 20. Frequency Noise Spectrum (Active/Regenerative ML)

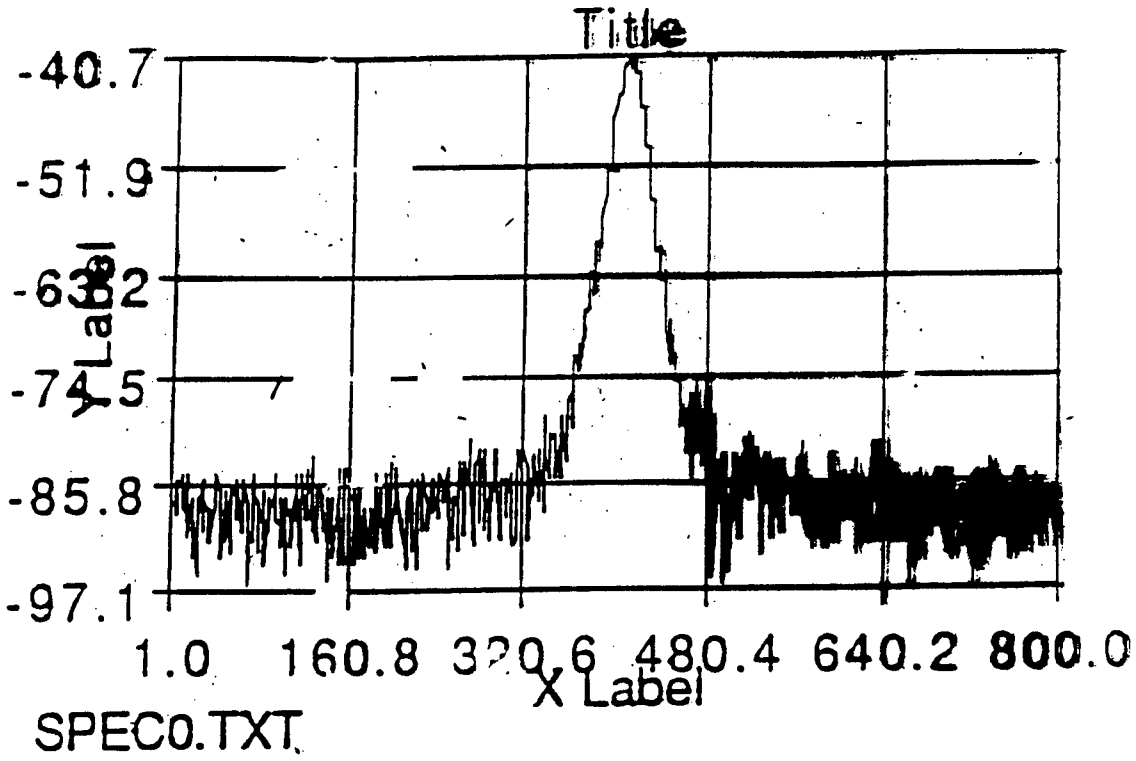

n= 8

SPEC2.TXT

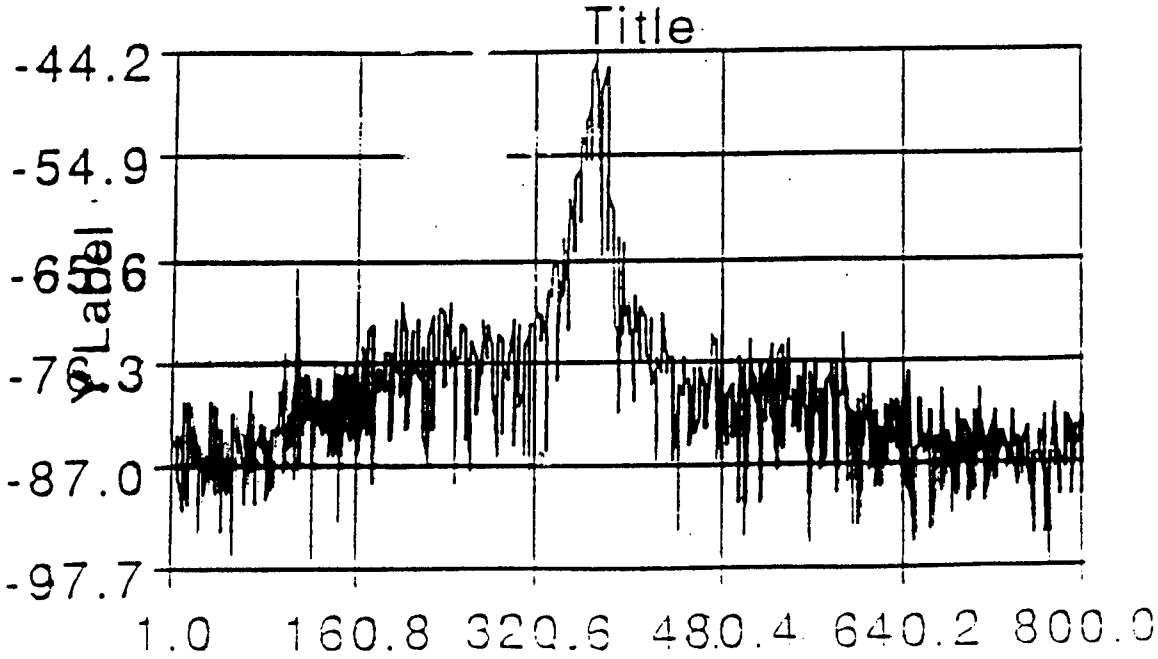

Figure 21. Frequency Noise Spectrum 8 th Harmonic

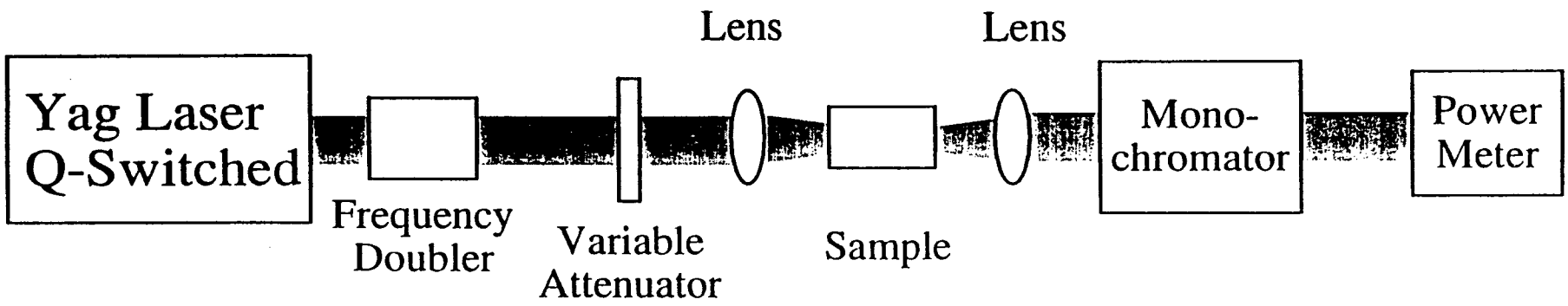

Raman Shift (1.06 to 1.54 μm) Experimental Setup

Figure 22. Raman Shift Experiment : Q Switched YAG Source

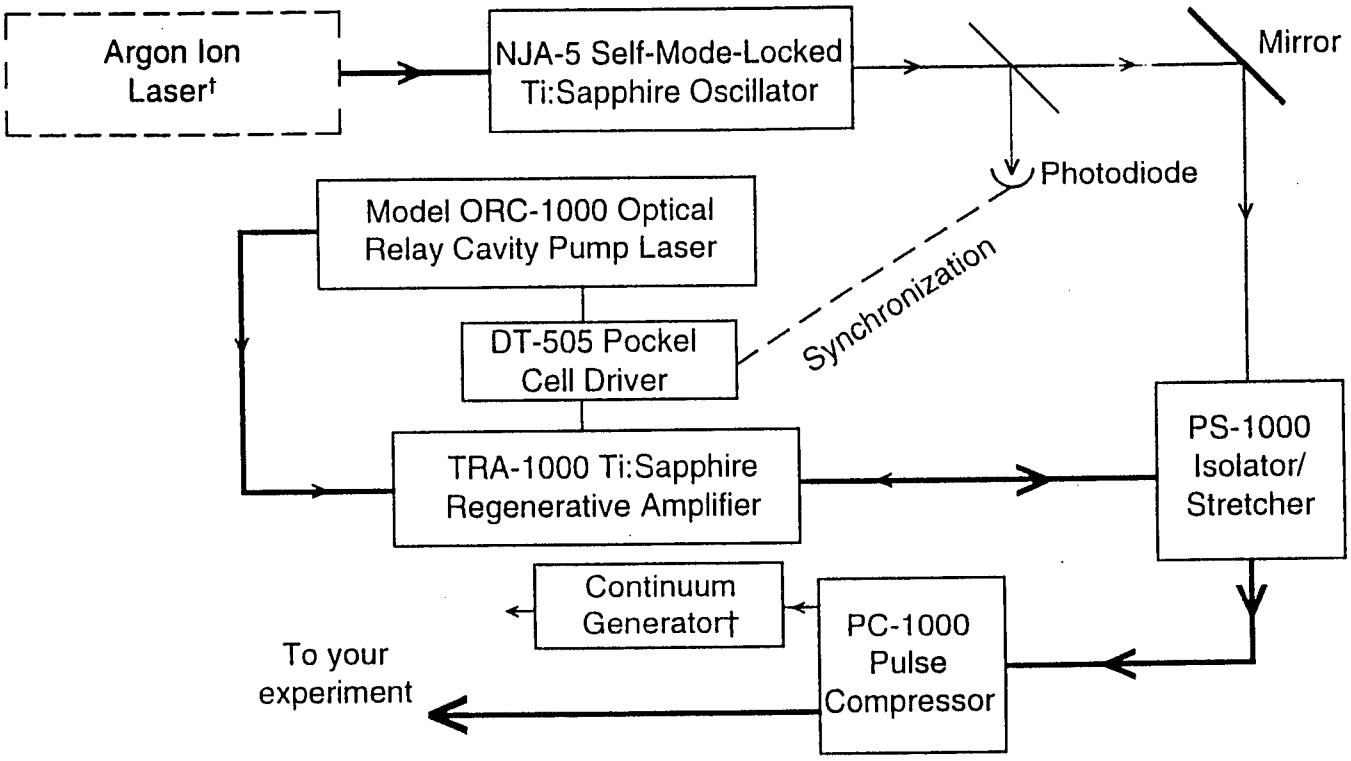

Figure 23. Femto-Second Ti Sapphire for Short Pulse Raman Test

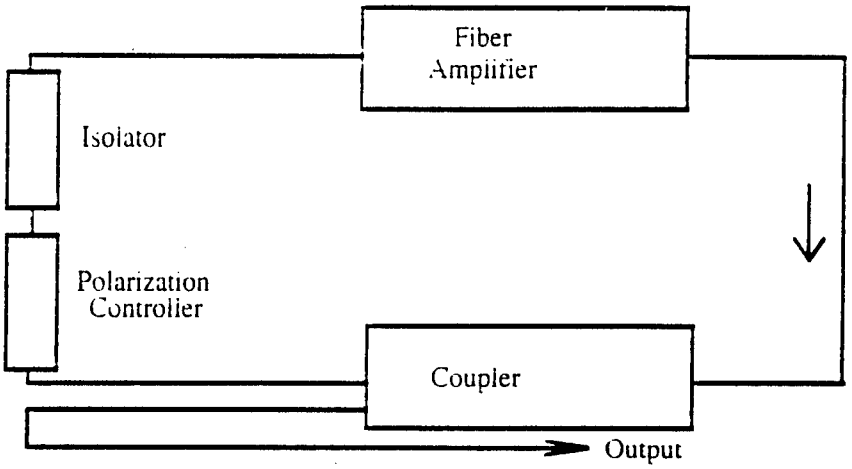

Figure 24. Passive Self-modelocked Fiber Laser #1

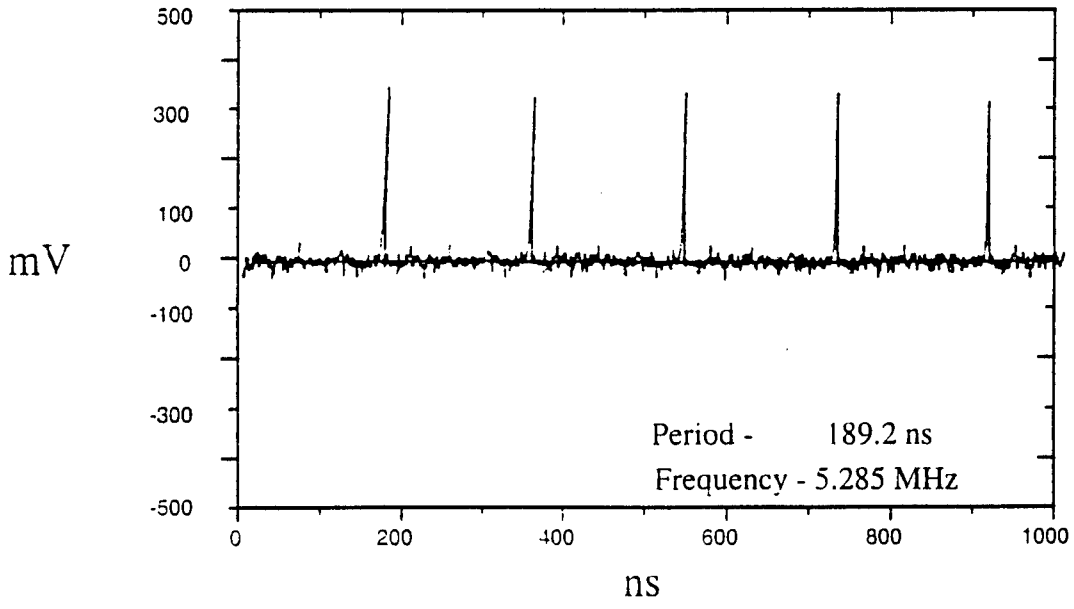

Figure 25. Oscilloscope Trace of Pulse Train

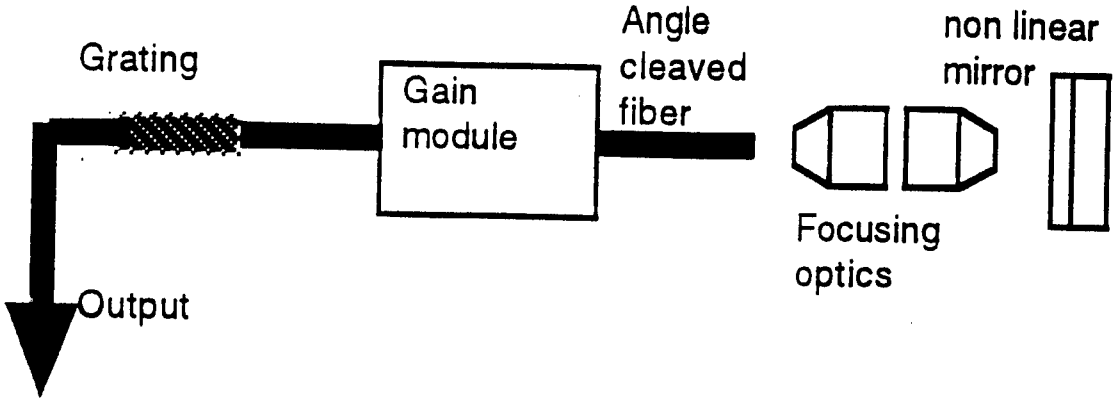

Lay out of mode locked laser

Figure 26. Passive Modelocked Laser #2

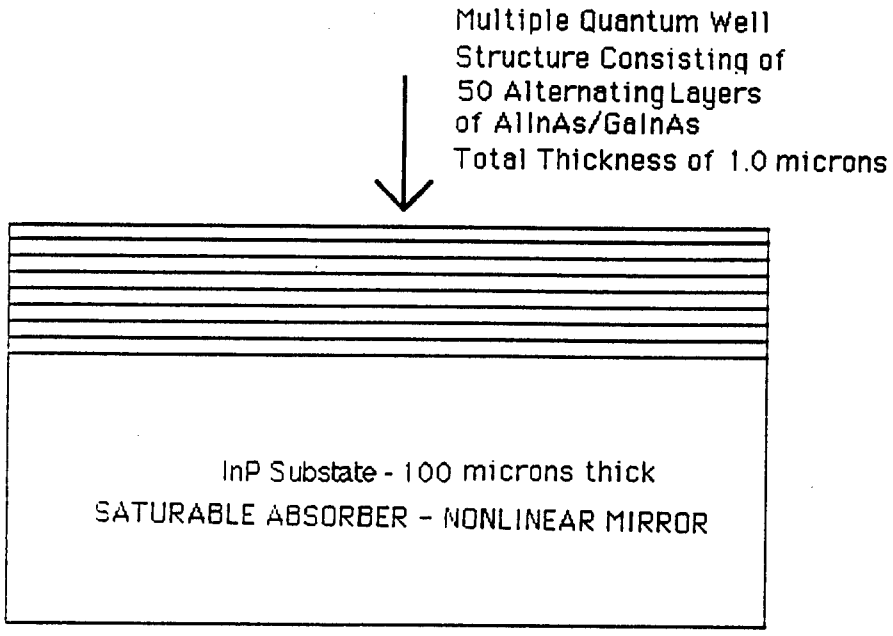

Figure 27. MQW Saturable Absorber Design

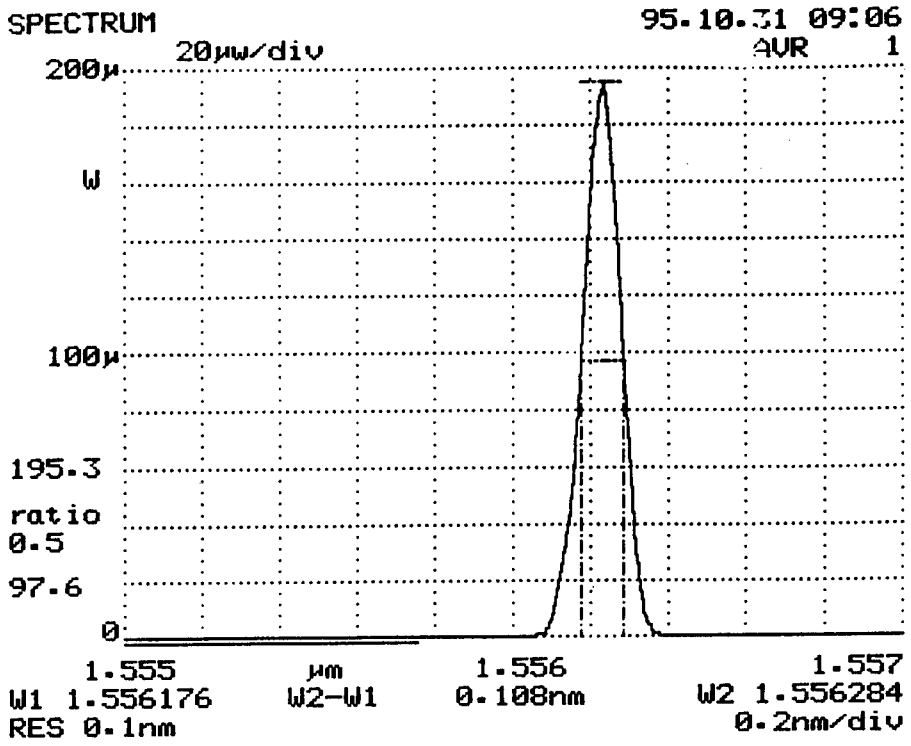

Figure 28. CW Optical Spectrum -- Fiber Laser #2

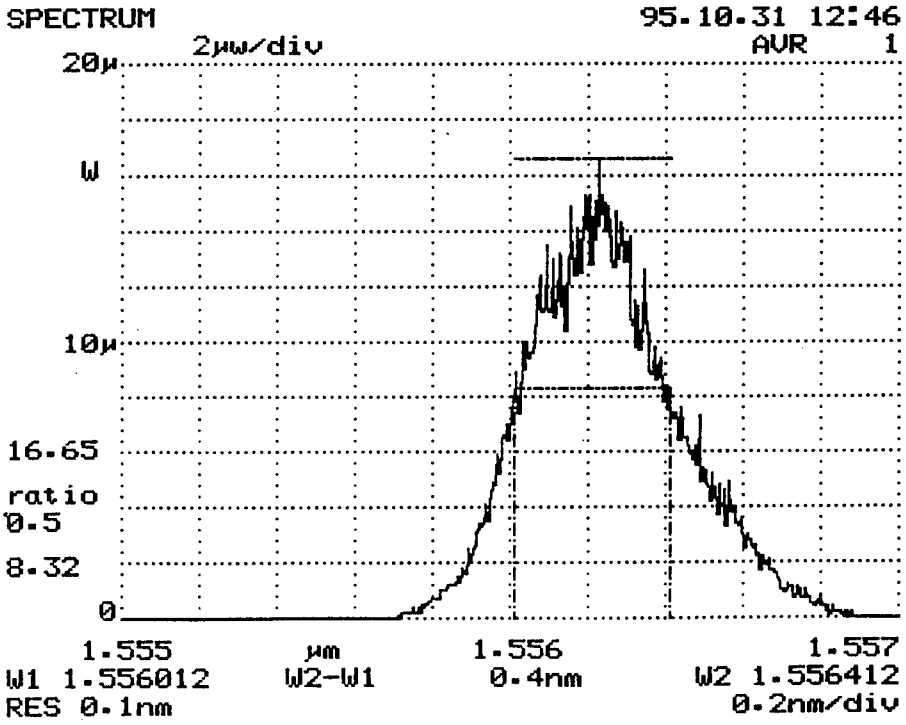

Figure 29. Modelocked Optical Spectrum -- Fiber Laser #2

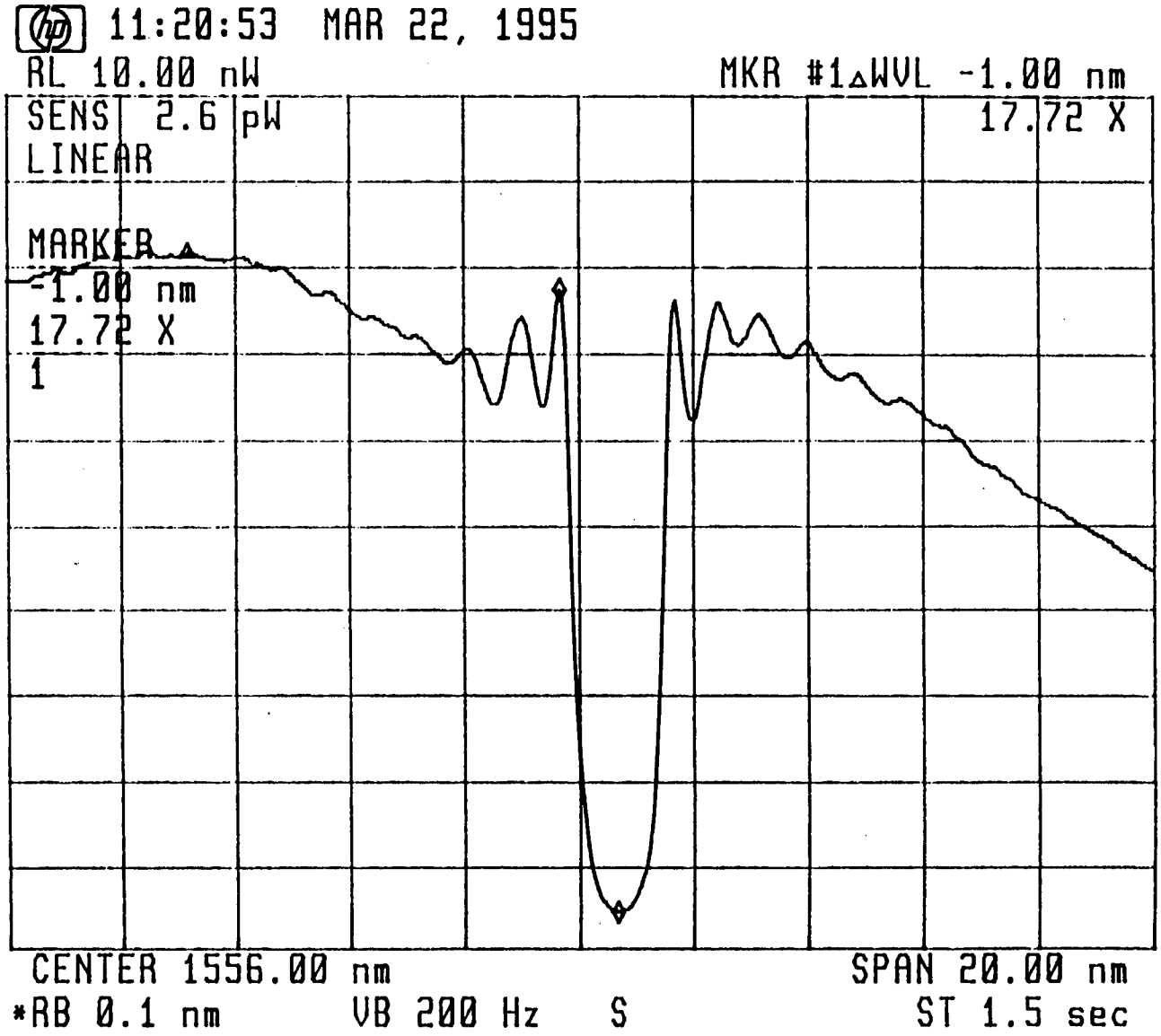

Figure 30. Spectral Trace of Fiber Bragg Grating

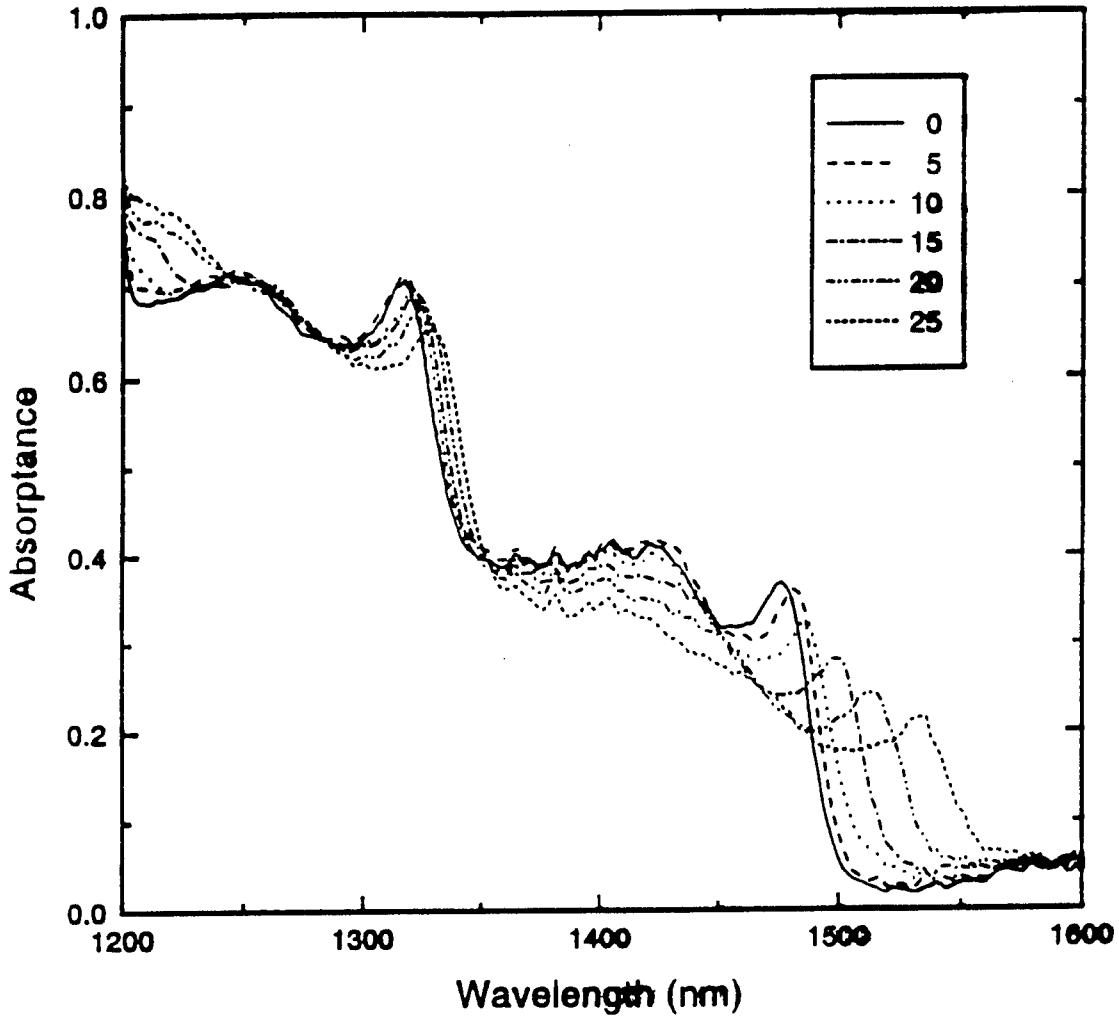

Figure 31. Spectral Trace of MQW S.A. Band Edge

ESTIMATION OF TEMPORAL INSTABILITY

$\Delta T = T/2\pi N [P_s * (\Delta \nu) / P_c B]$ *Ref.: von der Linde, 86*

T = Period
N = harmonic order
B = instrumental resolution
$\Delta \nu$ = 3 db bandwidth of sidebands
P_c = Power in carrier signal
P_s = Power in sideband noise

Results *ΔT (Active ML) = 0.8 Pico sec (approx)*

ΔT (Passive ML) = < 1 Picosec (contains causal noise)

SYNCHRONIZATION OBSERVATIONS

Injecting Active Fiber Laser into Passive _____ RESULTS

a) *Q- Switched / Modelocked behavior from Passive system*

b) *ΔT (jitter) = Not determined*

c) *Timing jitter is not necessarily transferred by injection*

d) *Q-Switching dominates the sideband noise*

e) *Pulse Energy 10 Nano joules (approx)*

Figure 32. Temporal Instability Test Results

MODELOCKING OBSERVATIONS

Active ML:

Pulse width	6 psec
Spectral	.4 nm

Transform Limited (Approx)
High Harmonics readily available (up to 120 th so far)

Passive ML:

Pulse Width	8 Psec
Spectral	0.2 nm
Time- Bandwidth	.31 indicates low residual dispersion
Pulse energy	0.8 nano Joule (approx)

"Nearly Self-Starting" Self starts modelocking from noise.
Otherwise; a perturbation of fiber or vibration required.

Independent of birefringence or polarization alignment.

* In general: Transient SELF Q- SWITCHING can precede pure modelocking.

Pulse width	70 nano sec (Approx)
Frequency:	0.8 Khz (Varies with pump power)

Figure 33. Modelocked Active/Passive Data Comparison

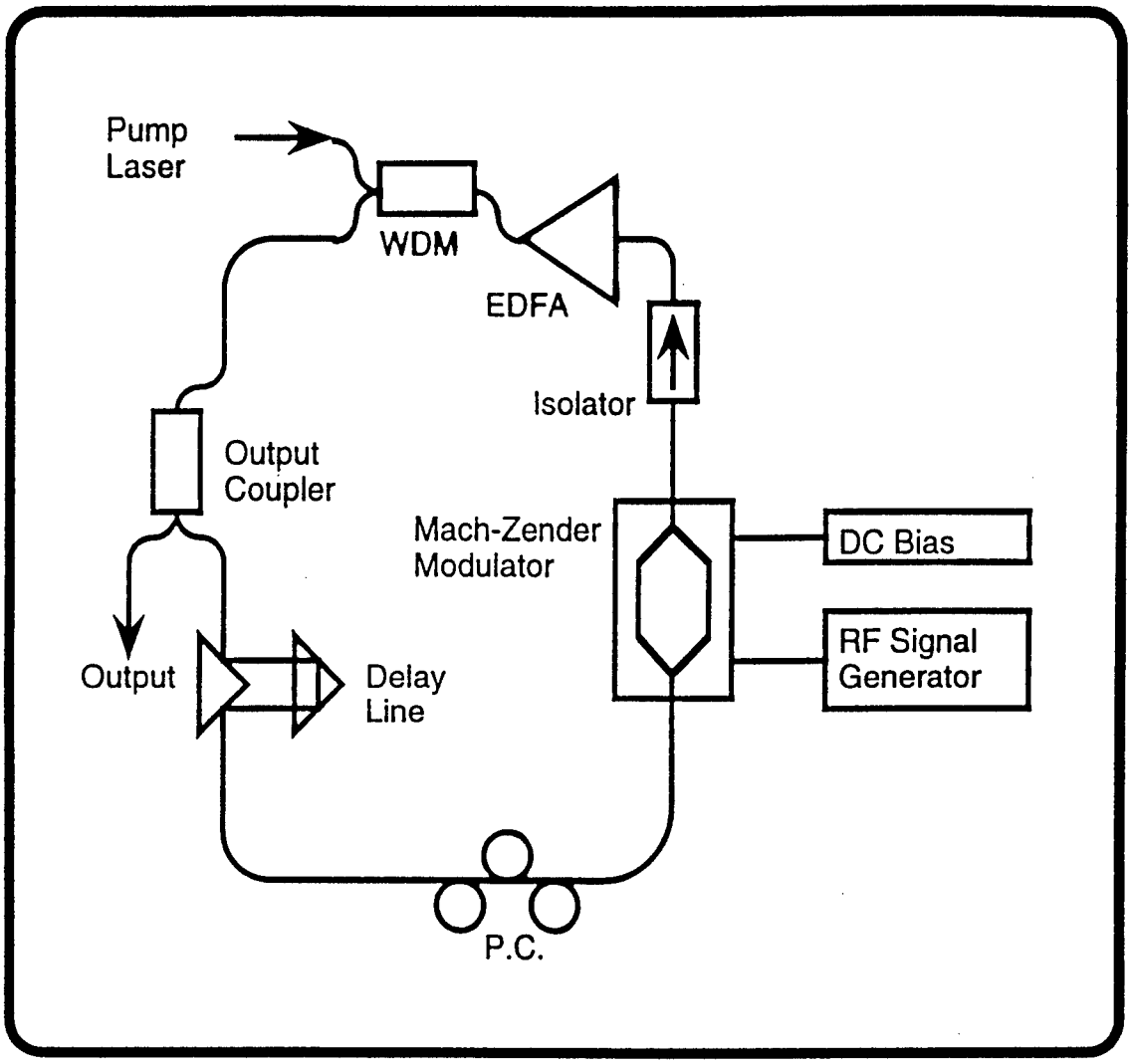

Figure 34. Layout of Actively Modelocked Fiber Laser

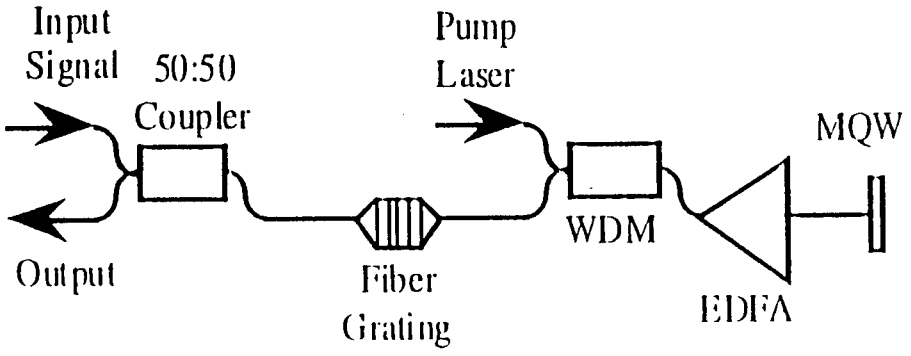

Figure 35. Laser #2 Configured for Synchronization

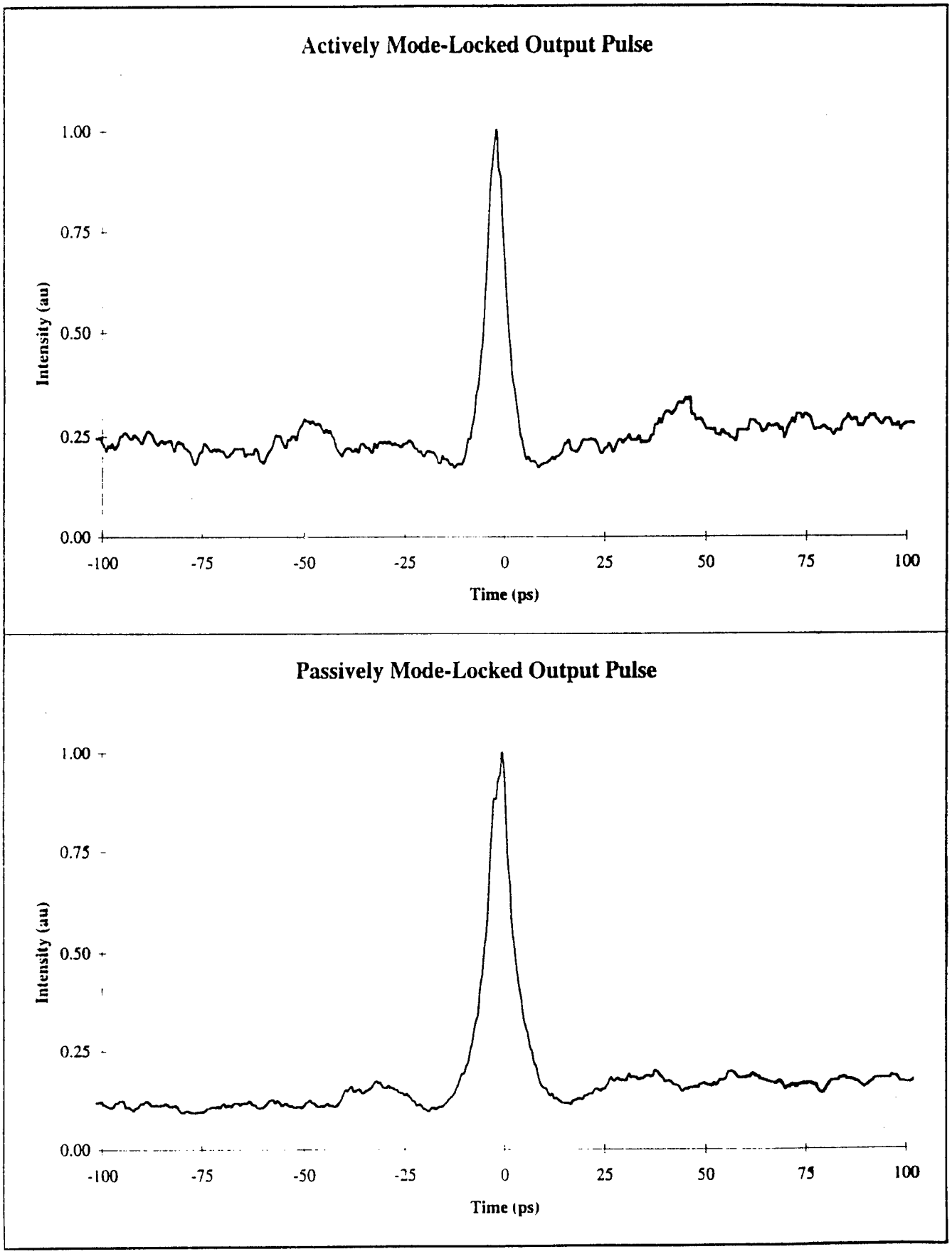

Figure 36. Autocorrelator Traces of Active /Passive Data

Synchronized Pulse Train

Figure 37. Synchronized Pulse Train-Scope Display

Figure 38. Fiber Tip Contact With MQW-Photo

Spectra of Tenth Harmonic Sideband

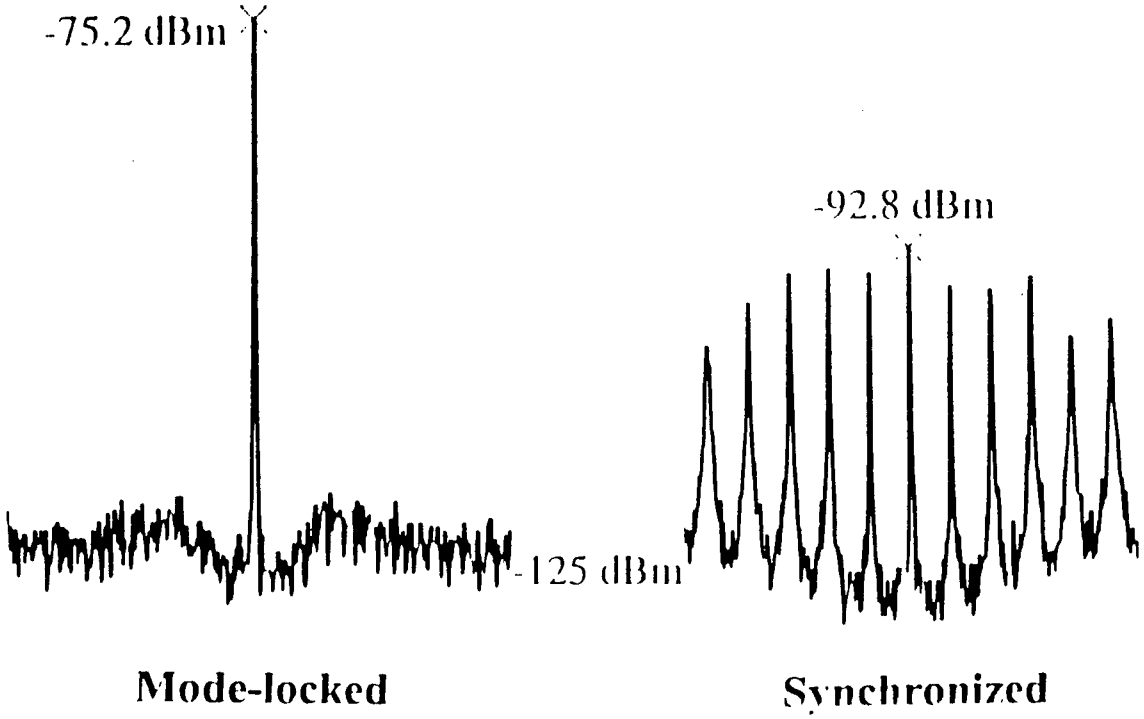

Figure 39. Microwave Noise Spectrum 10th Harmonic

*U.S. GOVERNMENT PRINTING OFFICE: 1997-509-127-47147